PHYSICAL REVIEW D **87,** 094016 (2013)

Top quark physics in the vector color-octet model

Sukanta Dutta,[1] Ashok Goyal,[2,*] and Mukesh Kumar[1,2,†]

[1]*SGTB Khalsa College, University of Delhi, Delhi 110007, India*

[2]*Department of Physics and Astrophysics, University of Delhi, Delhi 110007, India*

(Received 21 November 2012; published 15 May 2013)

We study and constrain the parameter space of the vector color-octet model from the observed data at the Tevatron by studying the top quark pair production and associated observables $A_{\mathrm{FB}}^{t\bar{t}}$ and spin correlation. In particular we study the invariant mass and rapidity dependence of $A_{\mathrm{FB}}^{t\bar{t}}$ at the Tevatron. In addition to the flavor conserving (FC) couplings we extend our study to include the flavor violating (FV) coupling involving the first and third generation quarks for both these processes. In order to ensure that we remain within the constraints imposed by the LHC data, we analyze the charge asymmetry, p_T spectrum and invariant mass in the $t\bar{t}$ production data at the LHC. The constraints from the dijet resonance searches performed by the LHC are also considered. We also explore the contribution of this model to the single top quark production mediated by charged and neutral color-octet vector bosons. FV couplings introduced then induce the same-sign top-pair production process which is analyzed for both the hadron colliders. We have incorporated the effect of finite decay width of color octets on these processes. We find that it is possible to explain the observed $A_{\mathrm{FB}}^{t\bar{t}}$ anomaly in the color-octet vector model without transgressing the production cross sections of all these processes both through FC and FV couplings at the Tevatron. We predict best point sets in the model parameter space for specific choices of color-octet masses corresponding to χ^2_{min} evaluated using the $m_{t\bar{t}}$ and $|\Delta y|$ spectrum of $A_{\mathrm{FB}}^{t\bar{t}}$ from the observed data set of Run II of the Tevatron at the integrated luminosity 8.7 fb^{-1}. We find that the single top quark production is more sensitive to the FC and FV couplings in comparison to the top-pair production. We provide 95% exclusion contours on the plane of FV chiral couplings from the recent data from Tevatron, CMS and ATLAS corresponding to the nonobservability of large same-sign dilepton events. The four observed point sets are consistent with the cross section, charge asymmetry and spin-correlation measurements for $t\bar{t}$ production and dijet searches at the LHC.

DOI: 10.1103/PhysRevD.87.094016 PACS numbers: 14.65.Ha, 12.60.−i, 13.85.Rm, 14.70.Pw

I. INTRODUCTION

Top quark production at high luminosity achieved at the recently shut down Tevatron has thrown tantalizing hints of physics beyond the Standard Model (SM). The combined analysis of the CDF and D0 collaborations has given results for top quark mass $m_t = 173.3 \pm 1.1$ GeV [1]. The current measured cross section from all channels with 4.6 fb^{-1} data is $\sigma^{t\bar{t}} = 7.5 \pm 0.31(\mathrm{stat}) \pm 0.34(\mathrm{syst}) \pm 0.15(\mathrm{Ztheory})\,\mathrm{pb}$ for $m_t = 172.5$ GeV [2]. For the same top mass the D0 collaboration reported $\sigma_{t\bar{t}} = 7.36^{+0.90}_{-0.79}(\mathrm{stat} + \mathrm{syst})$ pb using dilepton events [3]. The leading order process for $t\bar{t}$ production at the Tevatron is $q\bar{q} \to t\bar{t}$. The top-pair production cross section with the QCD corrections at the next-to-next-to-leading order (NNLO) level is computed to be $\sigma(t\bar{t})^{\mathrm{NNLO}}_{\mathrm{SM}} = 7.08^{+0.00+0.36}_{-0.24-0.27}$ pb for $m_t = 173$ GeV [4]. These corrections are not only significant but are also in agreement with the experiment.

The CDF and D0 collaborations have reported top quark forward-backward (FB) asymmetry $A_{\mathrm{FB}}^{t\bar{t}}$ for large $t\bar{t}$ invariant mass $m_{t\bar{t}}$ which shows a deviation of about two sigma from the SM prediction [5,6]. Recently CDF observed the parton level $A_{\mathrm{FB}}^{t\bar{t}}$ to be $0.296 \pm .067$ for $m_{t\bar{t}} > 450$ GeV based on the full Run II data set with luminosity of 8.7 fb^{-1} [7]. In the SM, this asymmetry arises only at the next to leading order through the interference between the Born term and higher order of QCD terms and is found to be 0.1 [8] which is too small to fit the data. In the literature the $A_{\mathrm{FB}}^{t\bar{t}}$ anomaly has been attributed to new physics (NP) beyond SM [9–12]. In this article we analyze the $m_{t\bar{t}}$ and $|\Delta y|$ distributions of $A_{\mathrm{FB}}^{t\bar{t}}$ induced by the color-octet vector bosons and compare with the distribution simulated from the observed data given in Ref. [7]. In light of the recent observations at the LHC, we constrain the new physics model parameter space from the invariant mass distribution of the $t\bar{t}$ production cross section and the measured associated charge asymmetry.

Single top quark production is an important process at hadron colliders in providing an opportunity to probe the electroweak (EW) interactions of the top quark. Although in the SM, single top quark is produced at the EW scale, it is noteworthy that the production cross section is comparable and only a little less than half of the $t\bar{t}$ pair production. The considerable background however makes

*agoyal45@yahoo.com
†mkumar@physics.du.ac.in

the extraction of the signal quite challenging. Recent analysis of the CDF collaboration uses 7.5 fb^{-1} of data and measures the single top quark total cross section of $\sigma_{s+t} = 3.04^{+0.57}_{-0.53}$ pb [13]. Using 5.4 fb^{-1} of collected data, D0 at the Fermilab Tevatron Collider measured the combined single top quark production cross section $\sigma_{s+t} = 3.43^{+0.73}_{-0.74}$ pb [14]. The predicted next-to-next-to-next-to-leading order (NNNLO) approximate calculation for both the modes are $\sigma_s = 0.523^{+0.001+0.030}_{-0.005-0.028}$ pb and $\sigma_t = 1.04^{+0.00}_{-0.02} \pm 0.06$ pb [4] for $m_t = 173$ GeV. Recently the CMS collaboration reported the t-channel EW single top quark cross section to be $83.6 \pm 29.8(\text{stat} + \text{syst}) \pm 3.3(\text{lumi})$ pb at $\sqrt{s} = 7$ TeV at the LHC [15] corresponding to integrated luminosity of 36 pb^{-1}, which agrees with the next-to-leading order (NLO) and resummation of collinear and soft-gluon corrections NNLO [4]. However the involved experimental and theoretical uncertainties allow us to explore the new physics consequences in the determination of the production cross section mediated by the new exotic vector bosons. Therefore it is worthwhile to study the effect of the couplings induced by the color-octet vector model in the s and t channel single top quark production.

The production of same-sign top quark pair is a fascinating process and would furnish unmistakable signature of physics beyond the SM. In the SM this process is highly suppressed and involves higher order flavor changing neutral current (FCNC) interactions. The search for the same-sign top quark pair involves searching for events with same-sign isolated leptons accompanied by hadron jets and missing transverse energy in the final sate. The CDF collaboration has set a limit on same-sign top-pair production at the Tevatron using a luminosity of 6.1 fb^{-1}, $\sigma(tt + \bar{t}\,\bar{t}) \times [\text{BR}(W \to l\nu)]^2 < 54$ fb with a 95% confidence level (CL) [16]. This limit puts severe constraints on physics beyond the SM which allows for FCNC interactions. The 7 TeV data from CMS also disfavors the same-sign top-pair production at the LHC mediated through Z' in t and u channels which otherwise was the potent model to explain the $A_{\text{FB}}^{t\bar{t}}$ anomaly observed in $t\bar{t}$ production at the Tevatron [17,18]. We probe the effect of the flavor violating couplings in the same-sign top-pair production both at the Tevatron and the LHC. These couplings are introduced to contest the $A_{\text{FB}}^{t\bar{t}}$ anomaly.

In Sec. II, we introduce the $\mathbf{3} \otimes \bar{\mathbf{3}}$ vector color-octet model. In Sec. III we compute the $t\bar{t}$ cross section and associated top quark forward-backward asymmetry $A_{\text{FB}}^{t\bar{t}}$ and spin-correlation coefficient in this model. Single top quark production is studied in Sec. IV and in Sec. V we probe the same-sign top quark production through flavor violating (FV) couplings. In Sec. VI we consider the constraints obtained by analyzing the LHC top quark data with reference to the resonance searches in $t\bar{t}$ production, dijet resonance searches and from the charge asymmetry data. Section VII is devoted to the discussion of the results and conclusion.

II. $3 \otimes \bar{3}$ VECTOR COLOR OCTETS

The exotic bosonic states that can couple to a quark (q) and antiquark ($\bar{q}$) pair in physics scenarios beyond the Standard Model are the scalar/vector color singlets, triplets, sextets and octets. Color singlet vector states are the Z's [19], W's [20], unparticles [9] and Kaluza-Klein gravitons G_{KK} [21]. Grinstein *et al.* [22] considered various scenarios of new physics models which contain scalars as well as vector representation of SM quark flavor symmetry group to study $t\bar{t}$ forward-backward anomaly and D0 dimuon anomaly at the Tevatron. They also studied the constraints on the flavor symmetric models and their collider signatures at the LHC with exotic bosons having masses around the electroweak scale.

Some of the colored exotic states are already present in some of theoretical models beyond the SM, for example R parity violating super-symmetric theories [23], excited quarks in composite models [24,25], diquarks in E_6 grand unified theories [26], in theories of extra dimension [27], color triplet and sextets [28] and in low scale string resonances [29]. Color-octet scalars have been studied in Ref. [30] while color-octet vector states coupled to $q\bar{q}$ are analyzed in Refs. [31,32] for axigluons and in Refs. [33–35] for colorons. Some of these exotic states have been involved in the literature to explain the top quark forward-backward asymmetry and the CDF dijet resonances. These particles if they exist can be produced at the LHC with their masses and couplings constrained by the measurement of the dijet cross section at the Tevatron and the LHC. The ATLAS and CMS collaborations [36] have reported stringent bounds on these colored states.

In this article, we investigate the contribution of color neutral and charged vector states $V_8^{0,\mu}$ and $V_8^{\pm,\mu}$ on $t\bar{t}$ production, top-quark forward-backward asymmetry, single top quark production and same-sign top-pair production. The interaction of color-octet vector states $V_8^{0,\pm,\mu}$ with quark is given by

$$\begin{aligned}\mathcal{L}_{q\bar{q}'V} = g_s[&V_8^{0a\mu}\bar{u}_i T^a \gamma_\mu (g_L^U P_L + g_R^U P_R) u_j \\ &+ V_8^{0a\mu}\bar{d}_i T^a \gamma_\mu (g_L^D P_L + g_R^D P_R) d_j \\ &+ (V_8^{+a\mu}\bar{u}_i T^a \gamma_\mu (C_L P_L + C_R P_R) d_j + \text{H.c.})]. \quad (1)\end{aligned}$$

Production of these color-octet resonants are studied in [37] where significant bounds for these resonances based on the preliminary CMS data have been obtained. We estimate the production event rates at a given luminosity for 200, 500, and 900 GeV vector color octets in Table I corresponding to the center of mass energy of 7, 8, and 14 TeV, respectively. For all these subprocesses the coupling constant of the octets with the light quarks along with the branching ratio are set to unity.

The color-octet vectors can be detected either through the resonant dijet and top-pair production. The measurement of the dijet events at the Tevatron and the LHC

TABLE I. Production event rate of the charged and neutral color-octet vector bosons for three different representative masses at three different collider energy and luminosity. To obtain these events we have set the product of the coupling constant squared and the branching fraction to unity.

$\sqrt{s}$ at LHC	$M_{V_8^{\pm,0}}$ GeV	N($u\bar{d} \to V_8^+$)	N($d\bar{u} \to V_8^-$)	N($u\bar{u} \to V_8^0$)	N($d\bar{d} \to V_8^0$)
7 TeV	200	2.2×10^8	1.2×10^8	2.1×10^8	1.3×10^8
$\mathcal{L} = 5$ fb^{-1}	500	8.1×10^6	3.5×10^6	7.0×10^6	4.2×10^6
	900	6.9×10^5	2.3×10^5	5.3×10^5	3.0×10^5
8 TeV	200	1.0×10^9	5.8×10^8	9.6×10^8	6.2×10^8
$\mathcal{L} = 20$ fb^{-1}	500	4.6×10^7	1.8×10^7	3.6×10^7	2.1×10^7
	900	3.7×10^6	1.3×10^6	3.0×10^6	1.7×10^6
14 TeV	200	9.9×10^9	6.0×10^9	9.6×10^9	6.3×10^9
$\mathcal{L} = 100$ fb^{-1}	500	4.6×10^8	2.4×10^8	4.3×10^8	2.6×10^8
	900	5.4×10^7	2.4×10^7	4.8×10^7	2.8×10^7

restricts the coupling of these exotic colored states to the light quark sector in the narrow resonance approximation (in units of $g_s = \sqrt{4\pi\alpha_s}$). However, the coupling of these states to the top quark sector essentially remains unexplored. It is to be noted that the $t\bar{t}$ cross section depends on the product of the couplings of V_8 with light and top quarks whereas the dijet cross section depends on the coupling of these exotics with light quarks only. We will revisit the resonant dijet production cross section in Sec. VI C.

Since there exist stringent constraints from flavor physics on FCNC, we consider nonuniversal FCNC couplings between the up quarks of the first and third generation only. However, after a rotation from weak eigenstates to mass eigenstates these FCNC interactions would contribute to B_q^0-$\bar{B}_q^0$ and D^0-$\bar{D}^0$ mixing. Consequently, by making a suitable choice of the left and right-handed mixing matrices along with the relevant couplings, we can evade the most restrictive constraint on these couplings from the low energy B and D phenomenology [38]. It has been discussed in the literature (see for example [39]) that in a scenario involving nonuniversal flavor coupling, if the generic flavor violation is confined to up quark sector and is so aligned as to induce minimal flavor violation, the constraints on color-octet vector boson with axial coupling of QCD strength from D-meson sector are rather weak, $M_{V_8^0} > 0.22$ TeV. The bounds on right-handed couplings are even weaker. On the other hand generic flavor violation in the down quark sector requires $M_{V_8^0}$ with axial couplings to be greater than several TeV from the neutral meson mixing data. Thus by keeping the u-t coupling large and simultaneously making c-t and u-c couplings small, we will not get any strong bounds from flavor physics. This reference also shows that the contribution to B_q^0-$\bar{B}_q^0$ mixing from the charge current sector can be controlled whenever the mixing matrices are aligned with the SM Cabibbo-Kobayashi-Maskawa resulting in the couplings $C_{L,R}$, $g_{L,R}$ naturally to be of the order one. Assuming minimal flavor violation breaking for a particular choice of flavor symmetry subgroup, authors of Ref. [22] were able to pinpoint the vector boson models consistent with FCNC constraints from B^0-$\bar{B}^0$ mixing and at the same time able to give right enhancement of $A_{\rm FB}^{t\bar{t}}$ for a benchmark point, say $M_{V_8^0} = 300$ GeV.

The couplings $g_{L,R}$ and $C_{L,R}$ are free parameters in our model and taken to be diagonal. $g_s = \sqrt{4\pi\alpha_s}$ is the QCD coupling; i, j are flavor indices and a represents the color index. We perform our calculations for top quark mass $m_t = 172.5$ GeV and bottom quark mass $m_b = 4.7$ GeV at the $p\bar{p}$ center of mass energy $\sqrt{s} = 1.96$ TeV, with fixed QCD coupling $\alpha_s = 0.13$ and using CTEQ6L1 parton distribution functions keeping factorization and renormalization scales $\mu_F = \mu_R = m_t$. We have incorporated the $\mathbf{3} \otimes \bar{\mathbf{3}}$ model in MadGraph/MadEvent V4 [40] and generated a total of 10000 events for all the processes. We do not take into account the effects from parton showering, hadronization and detector conditions in our studies.

The width of the new resonances are computed and taken into consideration for all the phenomenological observables presented in this study.

III. TOP-PAIR PRODUCTION

In this section we make a detailed study of $t\bar{t}$ production at the Tevatron to put bounds on the parameters of $\mathbf{3} \otimes \bar{\mathbf{3}}$ model. The new physics contribution to $t\bar{t}$ production in the present model arises through the exchange of flavor conserving and flavor violating neutral current (NC) V_8^0 as shown in Figs. 1(a) and 1(b), respectively. Here we assume that the flavor changing couplings are present only between the first and third generation quarks. We examine the sensitivity of both these couplings for the associated observables namely the forward-backward asymmetry and the spin-correlation coefficient along with the total production cross section.

At the Tevatron the $t\bar{t}$ pair is predominantly produced through the quark pair annihilation $q\bar{q} \to t\bar{t}$, where the quarks (antiquarks) are mainly moving along the proton

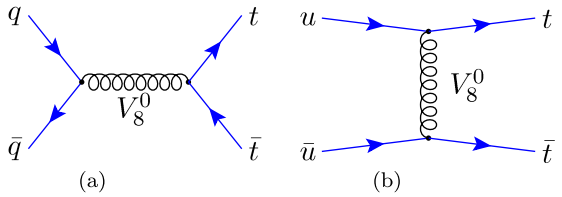

FIG. 1 (color online). Diagrams for $q\bar{q} \to t\bar{t}$ production through V_8^0 in (a) s-channel flavor conserving (FC) and (b) t-channel FV cases.

(antiproton) direction. The FB asymmetry can be defined as

$$A_{\rm FB} = \frac{N(\Delta y > 0) - N(\Delta y < 0)}{N(\Delta y > 0) + N(\Delta y < 0)}, \tag{2}$$

where N is the number of events and $\Delta y = y_t - y_{\bar{t}}$ is the difference in rapidities of top and the antitop quarks along the proton momentum direction in the lab frame. Recent measurements from the CDF and D0 collaborations at the Tevatron report positive asymmetries [5,6], $A_{\rm FB}^{\rm CDF} = 0.158 \pm 0.075$, $A_{\rm FB}^{\rm D0} = 0.196 \pm 0.065$ at the subprocess/parton level after correcting for backgrounds and detector effects corresponding to integrated luminosity of 5.3 and 5.4 fb^{-1}, respectively, whereas the SM prediction at NLO QCD level is 0.051 [41]. A recent report from CDF, studied FB asymmetry and its mass and rapidity dependence with an integrated luminosity of 8.7 fb^{-1} at the Tevatron resulting in an inclusive parton level $A_{\rm FB} = 0.162 \pm 0.047$ [7].

Spin correlation of the top-antitop pair, in the "helicity basis," (i.e., choosing the direction of the top quark momentum as our spin quantization axis) is described by four independent helicity states $\bar{t}_L t_R$, $\bar{t}_R t_L$, $\bar{t}_L t_L$, $\bar{t}_R t_R$. The spin-correlation parameter is defined as

$$C^{t\bar{t}} = \frac{[\sigma(\bar{t}_R t_L) + \sigma(\bar{t}_L t_R)] - [\sigma(\bar{t}_R t_R) + \sigma(\bar{t}_L t_L)]}{[\sigma(\bar{t}_R t_L) + \sigma(\bar{t}_L t_R)] + [\sigma(\bar{t}_R t_R) + \sigma(\bar{t}_L t_L)]} = \frac{N_O - N_S}{N_O + N_S}, \tag{3}$$

where $N_S = \Uparrow\Uparrow + \Downarrow\Downarrow$ and $N_O = \Uparrow\Downarrow + \Downarrow\Uparrow$ are the number of top and antitop quarks with their spins parallel and antiparallel, respectively. Recent studies have shown strong spin correlation in the top quark pair production which means that the top quark and antiquark have preferential spin polarizations. At the Tevatron the dominant parton level top-pair production is $q\bar{q} \to t\bar{t}$ and its value for the SM in the helicity basis is 0.299 [42]. CDF reported the measurement of the spin-correlation coefficient $C^{t\bar{t}}_{\rm helicity} = 0.60 \pm 0.50({\rm stat}) \pm 0.16({\rm syst})$ [43] in the helicity basis and $0.042^{+0.563}_{-0.562}$ [44] in the beam basis. Any deviation in the measurement of $C^{t\bar{t}}$ would give an indirect idea of the new $t\bar{t}$ production mechanism and also models of new physics appeal to the spin correlation for signal identification and discrimination [45–49].

A. Flavor conserving

The additional Feynman diagrams induced by the color-octet vector bosons depicted in Fig. 1, interfere with the SM tree annihilation process. We take the color-octet vector boson couplings with the first two generations, i.e., light quarks g_i^q ($q = u, d, s, c$) to be typically an order of magnitude smaller than the third generation heavy quarks $g_i^{t,b}$ with $i, j = L/R$. This is consistent with the dijet measurements at the Tevatron. The corresponding NP matrix element is proportional to the product of light and heavy quarks couplings. For convenience we choose the product of two couplings $\sqrt{\lambda_{ij}} = \sqrt{g_i^q g_j^t}$ and the mass $M_{V_8^0}$ as a parameter of our model in the FC case. Since the total matrix element squared is left-right symmetric, we have only three independent choices of the combinations of couplings which includes the (a) vector, (b) axial-vector and (c) right-chiral interactions. All three cases can be explicitly expressed as

$$\begin{aligned}
&(a)\,\text{Vector: } g_L^q = g_R^q, g_L^t = g_R^t, \\
&\qquad \Rightarrow \lambda_{LL} = \lambda_{RR} = \lambda_{RL} = \lambda_{LR} = \lambda_{VV} \\
&(b)\,\text{Axial vector: } g_L^q = -g_R^q, g_L^t = -g_R^t, \\
&\qquad \Rightarrow \lambda_{LL} = \lambda_{RR} = -\lambda_{RL} = -\lambda_{LR} = \lambda_{AA} \\
&\qquad \text{or } \; g_L^q = -g_R^q, g_R^t = -g_L^t \\
&\qquad \text{or } \; g_R^q = -g_L^q, g_L^t = -g_R^t, \\
&\qquad \Rightarrow -\lambda_{LL} = -\lambda_{RR} = \lambda_{RL} = \lambda_{LR} = \lambda_{NA} \\
&(c)\,\text{Right chiral: } g_L^q = g_L^t = 0, \\
&\qquad \Rightarrow \lambda_{LL} = \lambda_{LR} = \lambda_{RL} = 0 \neq \lambda_{RR}.
\end{aligned}$$

These massive color octets are likely to decay to the lighter quarks as well as to the heavier one if kinetically allowed both through the flavor conserving as well as flavor violating couplings. The nonzero decay width for the heavy color octets can have appreciable effects not only in the $t\bar{t}$ cross section but also in the observables like $A_{\rm FB}^{t\bar{t}}$ and $C^{t\bar{t}}$. The decay width of color-octet vector boson is given by

$$\Gamma_{V_8} = \frac{1}{6}\alpha_s \left[(g_L^2 + g_R^2)\left\{ \frac{M_{V_8}^2}{2} - \frac{m_q^2 + m_{q'}^2}{4} - \left(\frac{m_q^2 - m_{q'}^2}{2M_{V_8}}\right)^2 \right\} + 3 m_q m_{q'} g_L g_R \right] \frac{\lambda^{\frac{1}{2}}(M_{V_8}^2, m_q^2, m_{q'}^2)}{M_{V_8}^3}, \tag{4}$$

where $\lambda(x, y, z) = x^2 + y^2 + z^2 - 2x \cdot y - 2y \cdot z - 2z \cdot x$. In the flavor conserving case, for $M_{V_8} \leq 2m_t$, $q(= q') = u$, d, s, c, b while for $M_{V_8} \geq 2m_t$ top quarks also contribute. The only flavor violating mode we have is $V_8^0 \to u\bar{t} + \bar{u}t$. The decay of the charged color-octet vector boson $V_8^{\pm} \to qq'$ proceeds through the exotic charge current (CC) interactions which are assumed to diagonal but with non-universal coupling to the third generation quark sector.

Throughout our analysis we have taken into account the effect of the finite decay width in evaluating the cross sections and other associated observables.

The analytical expression of differential cross section in terms of λ_{ij} for $q\bar{q} \to t\bar{t}$ with respect to the cosine of the top quark polar angle θ in the $t\bar{t}$ center-of-mass (c.m.) frame is given as

$$\frac{d\hat{\sigma}}{d\cos\theta} = \frac{\pi\beta\alpha_s^2}{9\hat{s}}\Bigg[f(\theta,\beta^2) + \Bigg\{\left(1-\frac{M_{V_8^0}^2}{\hat{s}}\right)^2 + \frac{M_{V_8^0}^2}{\hat{s}}\frac{\Gamma_{V_8^0}^2}{\hat{s}}\Bigg\}^{-1}\Bigg\{(\lambda_{LR}^2+\lambda_{RL}^2+\lambda_{LL}^2+\lambda_{RR}^2)(2-\sin^2\theta)\frac{\beta^2}{4}$$
$$+ ((\lambda_{LL}+\lambda_{LR})^2+(\lambda_{RL}+\lambda_{RR})^2)\frac{1-\beta^2}{4} + \frac{1}{2}\left(1-\frac{M_{V_8^0}^2}{\hat{s}}\right)(\lambda_{LL}+\lambda_{RR}+\lambda_{LR}+\lambda_{RL})f(\theta,\beta^2)$$
$$+ \left(\left(1-\frac{M_{V_8^0}^2}{\hat{s}}\right)(\lambda_{LL}+\lambda_{RR}-\lambda_{LR}-\lambda_{RL}) + \frac{1}{4}(\lambda_{LL}^2+\lambda_{RR}^2-\lambda_{LR}^2-\lambda_{RL}^2)\right)\beta\cos\theta\Bigg\}\Bigg], \tag{5}$$

where $\hat{s} = (p_q + p_{\bar{q}})^2$ is the squared c.m. energy of the system, $\beta = \sqrt{1-4m_t^2/\hat{s}}$ is the top quark velocity and $f(\theta,\beta^2) = (2-\beta^2\sin^2\theta)$. The terms proportional to $\cos\theta$ in Eq. (5) are sensitive to the forward backward asymmetry. In Figs. 2–4 we plot the variation of the cross section, the forward backward asymmetry $A_{\rm FB}^{t\bar{t}}$ and the spin correlation $C_{t\bar{t}}$, respectively, as a function of coupling $\sqrt{\lambda_{ij}}$.

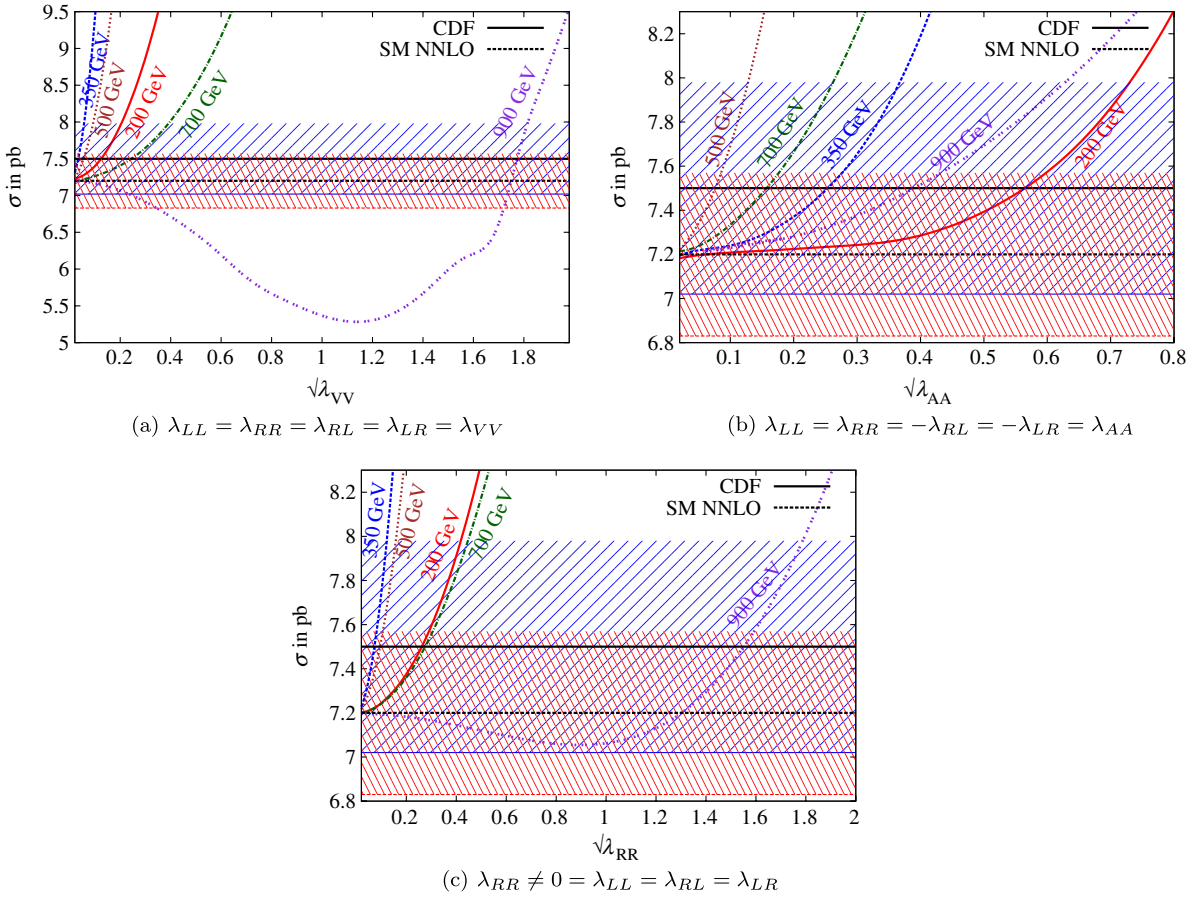

(a) $\lambda_{LL} = \lambda_{RR} = \lambda_{RL} = \lambda_{LR} = \lambda_{VV}$

(b) $\lambda_{LL} = \lambda_{RR} = -\lambda_{RL} = -\lambda_{LR} = \lambda_{AA}$

(c) $\lambda_{RR} \neq 0 = \lambda_{LL} = \lambda_{RL} = \lambda_{LR}$

FIG. 2 (color online). Variation of the cross section $\sigma(p\bar{p} \to t\bar{t})$ with couplings $\sqrt{\lambda_{ij}}$ for flavor conserving vector color octets corresponding to different values of $M_{V_8^0}$. The upper black dotted line associated with a blue band depicts the cross section 7.50 ± 0.48 pb from CDF (all channels) [3], while the lower black dot-dashed line associated with a red band show theoretical estimate 7.2 ± 0.37 pb at NNLO [4]. (a), (b), and (c) show the variation of σ for vector, axial and right-handed cases, respectively, [the cases (a), (b), and (c) as in the text].

We look at three different regions based on the octet masses and the threshold of top-pair production, region I where $M_{V_8^0} \ll 2m_t$, region II $M_{V_8^0} - \Gamma_{V_8^0} \leq 2m_t \leq M_{V_8^0} + \Gamma_{V_8^0}$ and region III where $M_{V_8^0} \gg 2m_t$, respectively. Figure 2(a) corresponds to the case (a), which implies pure vector interactions. For $M_{V_8^0} = 200$ GeV which lies in region I, the cross section grows with coupling due to the positive interference in spite of the s-channel suppression. For $M_{V_8^0} = 350$–500 GeV which lies in the resonant region II, we have a much sharper rise in the cross section with the increasing coupling. For higher octet masses we observe the effect of negative interference with SM as long as the coupling $|\lambda_{ij}| \leq 1$ and then it gradually grows with the couplings due to the dominance of the new physics squared term. However, pure vector interactions fail to generate the $A_{\rm FB}^{t\bar{t}}$.

Figure 2(b) corresponds to phenomenologically interesting case (b), which is purely an axial interaction and thus generates a large forward-backward asymmetry. Since the interference terms contributing to the cross section vanish in this case and only the squared term grows with coupling, we observe that this generates an increasing $A_{\rm FB}^{t\bar{t}}$ without enhancing the cross section for the couplings $|\lambda_{ij}| \leq 1$. However for the higher masses in region III, the $A_{\rm FB}^{t\bar{t}}$ becomes negative due to the negative interference with SM as shown in Fig. 3(b).

The fair amount of $A_{\rm FB}^{t\bar{t}}$ can also be generated through axial current for large masses by taking the negative product of the axial couplings of the light quark and the top quark, keeping the cross section the same as before. We depict the $A_{\rm FB}^{t\bar{t}}$ contribution for the negative product of axial couplings in Fig. 3(a).

The variation of the cross section for case (c) is given in Fig. 2(c) which is similar to case (a). In this case we get positive $A_{\rm FB}$ for all the cases but it grows faster for $M_{V_8^0} = 500$ GeV with respect to $\sqrt{\lambda_{RR}}$ comparing to other two masses of V_8^0 as shown in Fig. 3(c).

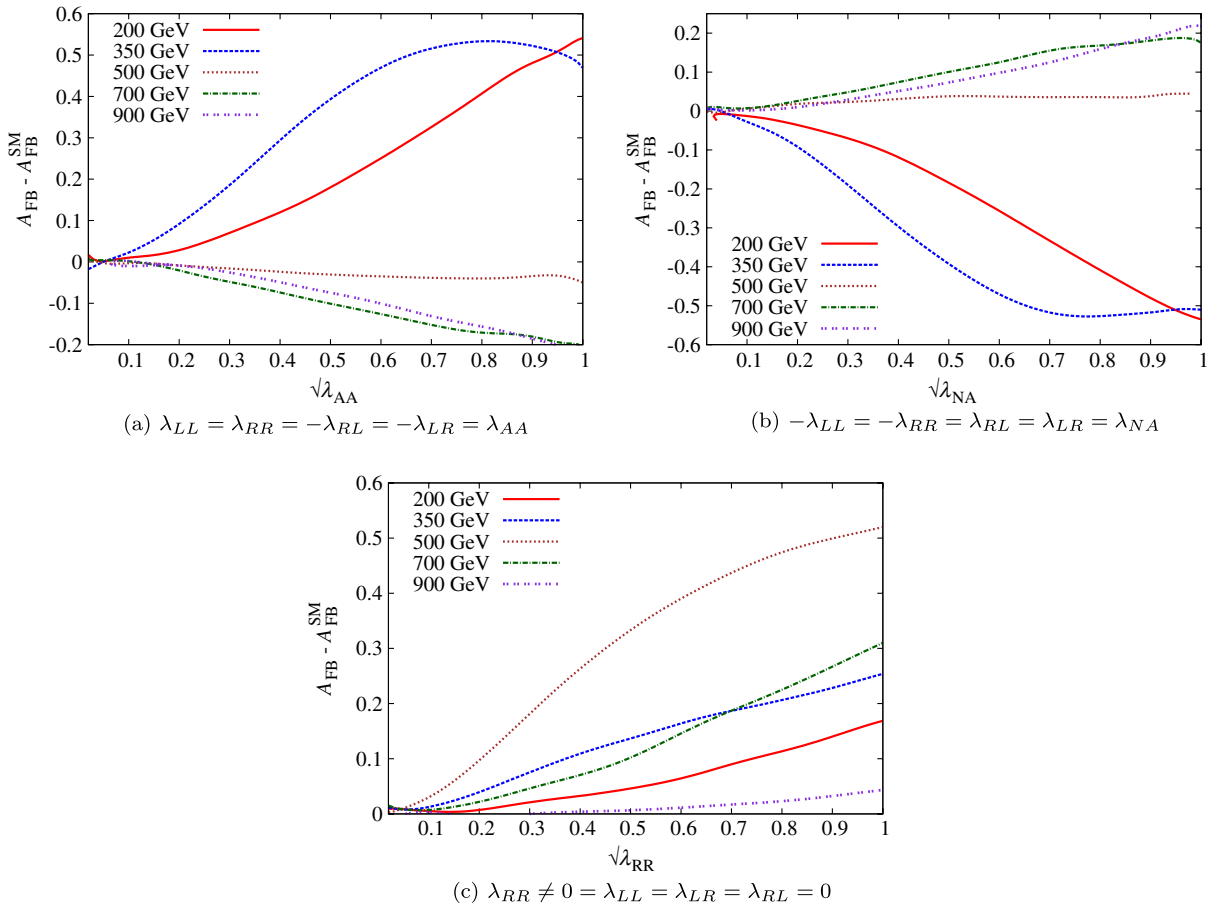

(a) $\lambda_{LL} = \lambda_{RR} = -\lambda_{RL} = -\lambda_{LR} = \lambda_{AA}$

(b) $-\lambda_{LL} = -\lambda_{RR} = \lambda_{RL} = \lambda_{LR} = \lambda_{NA}$

(c) $\lambda_{RR} \neq 0 = \lambda_{LL} = \lambda_{LR} = \lambda_{RL} = 0$

FIG. 3 (color online). Variation of the $A_{\rm FB} - A_{\rm FB}^{\rm SM}$ with couplings $\sqrt{\lambda_{ij}}$ for flavor conserving vector color octets corresponding to different values of $M_{V_8^0}$. (a), (b), and (c) correspond to the positive product of axial couplings, negative product of axial couplings and purely right-handed cases (the first two corresponds to cases (b) and the third corresponds to case (c) in the text, respectively). The $A_{\rm FB}^{t\bar{t}}$ for case (a) vanishes identically for all mass regions.

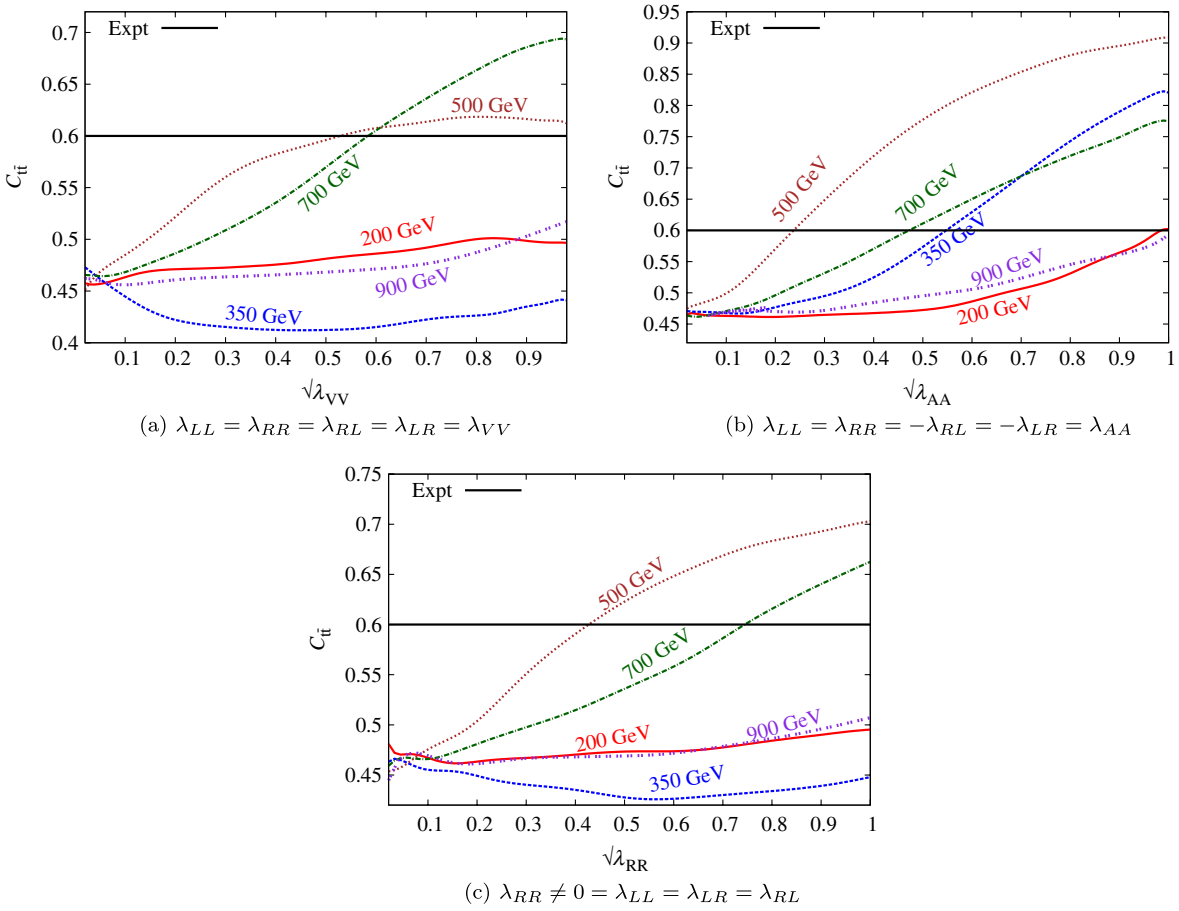

(a) $\lambda_{LL} = \lambda_{RR} = \lambda_{RL} = \lambda_{LR} = \lambda_{VV}$ (b) $\lambda_{LL} = \lambda_{RR} = -\lambda_{RL} = -\lambda_{LR} = \lambda_{AA}$

(c) $\lambda_{RR} \neq 0 = \lambda_{LL} = \lambda_{LR} = \lambda_{RL}$

FIG. 4 (color online). Variation of the spin-correlation coefficient $C^{t\bar{t}}$ with couplings $\sqrt{\lambda_{ij}}$ for flavor conserving vector color octets corresponding to different values of $M_{V_8^0}$. (a), (b), and (c) correspond to vector, axial and right-handed cases, respectively, (cases (a), (b), and (d) in the text, respectively). The spin-correlation variation for cases (c) and (b) as in text are identical.

The behavior of the variation of the spin-correlation coefficients can be understood by exhibiting the total matrix element squared as a combination of the same and opposite helicity amplitudes. The differential cross sections corresponding to the same and opposite helicity amplitudes are

$$\frac{d\hat{\sigma}_S^{\mathrm{FC}}}{d\cos\theta} = g_s^4(1-\beta^2)\sin^2\theta\left[8 + \frac{2\hat{s}(\hat{s}-M_{V_8^0}^2)}{(\hat{s}-m_{V_8^0}^2)^2+\Gamma_{V_8^0}^2 M_{V_8^0}^2}(\lambda_{LL}+\lambda_{RR}+\lambda_{LR}+\lambda_{RL}) + \frac{\hat{s}^2}{(\hat{s}-M_{V_8^0}^2)^2+\Gamma_{V_8^0}^2 M_{V_8^0}^2}(\lambda_{LL}^2+\lambda_{RR}^2+\lambda_{LR}^2+\lambda_{RL}^2+2(\lambda_{LL}\lambda_{LR}+\lambda_{RL}\lambda_{RR}))\right], \tag{6}$$

$$\begin{aligned}\frac{d\hat{\sigma}_O^{\mathrm{FC}}}{d\cos\theta} &= g_s^4(1+\cos^2\theta)\left[8+\frac{\hat{s}(\hat{s}-M_{V_8^0}^2)}{(\hat{s}-M_{V_8^0}^2)^2+\Gamma_{V_8^0}^2 M_{V_8^0}^2}(\lambda_{LL}+\lambda_{RR}+\lambda_{LR}+\lambda_{RL})\right.\\ &\left.+\frac{\hat{s}^2}{(\hat{s}-M_{V_8^0}^2)^2+\Gamma_{V_8^0}^2 M_{V_8^0}^2}\{(1+\beta^2)(\lambda_{LL}^2+\lambda_{RR}^2+\lambda_{LR}^2+\lambda_{RL}^2)+2(1-\beta^2)(\lambda_{LL}\lambda_{LR}+\lambda_{RL}\lambda_{RR})\}\right]\\ &+ g_s^4(2\beta\cos\theta)\left[\frac{\hat{s}(\hat{s}-M_{V_8^0}^2)}{(\hat{s}-M_{V_8^0}^2)^2+\Gamma_{V_8^0}^2 M_{V_8^0}^2}(\lambda_{LL}+\lambda_{RR}-\lambda_{LR}-\lambda_{RL})+\frac{\hat{s}^2}{(\hat{s}-M_{V_8^0}^2)^2+\Gamma_{V_8^0}^2 M_{V_8^0}^2}2(\lambda_{LL}^2+\lambda_{RR}^2-\lambda_{LR}^2-\lambda_{RL}^2)\right].\end{aligned} \tag{7}$$

Examining Eqs. (6) and (7), we find that for case (a), the contribution from the $\frac{d\hat{\sigma}_S^{FC}}{d\cos\theta}$ is suppressed by the factor $(1-\beta^2)\sin^2\theta/(1+\cos^2\theta)$ with respect to $\frac{d\hat{\sigma}_O^{FC}}{d\cos\theta}$, while for the case (b), only new physics squared term from $\frac{d\hat{\sigma}_O^{FC}}{d\cos\theta}$ contributes to the spin-correlation coefficient. For the right-chiral current case (c), we observe that for the interference term the ratio is again suppressed by the same factor as in case (a), while it is further suppressed by the factor $1/(1+\beta^2)$ for the squared term. Therefore it is evident that $C^{t\bar{t}}$ is likely to increase with the increasing coupling products.

A variation of spin-correlation coefficient $C^{t\bar{t}}$ with respect to $\sqrt{\lambda_{ij}}$ has almost similar behavior for all the cases considered as shown in Figs. 4(a)–4(c). Here the $C^{t\bar{t}}$ in region I first decreases with couplings due to negative interference and then increases due to the dominance of the squared term. For the octet mass 350 GeV at the region II the $C^{t\bar{t}}$ registers the minimum value showing that at threshold production it is likely to have an equal number of parallel and antiparallel states. In axial cases (b) and (c), since there is no interference, the $C^{t\bar{t}}$ increases with couplings for all mass regions which is evident from Fig. 4(b).

B. Flavor violating

In the flavor violating case, apart from the usual SM diagrams we have t-channel diagrams for $u\bar{u}\to t\bar{t}$ with V_8^0 as shown in Fig. 1(b) which interfere with the corresponding s-channel SM diagrams initiated with u and $\bar{u}$ partons. The flavor violating neutral coupling is considered only among the first and third generation u and t quarks g_i^{ut} $(i=L,R)$ with V_8^0. In contrast to the flavor conserving case, here we consider only two choices of coupling combinations (a) $g_L^{ut}=g_R^{ut}$ or $g_L^{ut}=-g_R^{ut}$ and (b) $g_L^{ut}=0$ or $g_R^{ut}=0$ to study the three observables because corresponding matrix element square is symmetric in both the cases. The differential cross section in terms of flavor violating neutral coupling g_i^{ut} for $u\bar{u}\to t\bar{t}$ with QCD s-channel and additional t-channel diagrams through V_8^0 (NP) with respect to the cosine of the top quark polar angle θ in the $t\bar{t}$ c.m. frame is

$$\frac{d\hat{\sigma}}{d\cos\theta}=\frac{\pi\beta\alpha_s^2}{9\hat{s}}(2-\beta^2\sin^2\theta)-\frac{\pi\beta\alpha_s^2}{54\hat{s}^2}\frac{\hat{s}^2(\hat{t}-M_{V_8^0}^2)}{(\hat{t}-M_{V_8^0}^2)^2+\Gamma_{V_8^0}^2M_{V_8^0}^2}(1+\beta\cos\theta)^2(g_L^{ut2}+g_R^{ut2})$$
$$+\frac{\pi\beta\alpha_s^2}{36\hat{s}}\frac{\hat{s}^2}{(\hat{t}-M_{V_8^0}^2)^2+\Gamma_{V_8^0}^2M_{V_8^0}^2}[(g_L^{ut4}+g_R^{ut4})(1+\beta\cos\theta)^2+8g_L^{ut2}g_R^{ut2}(1+\beta^2)], \quad (8)$$

where $\hat{t}=(p_u-p_t)^2=(p_{\bar{u}}-p_{\bar{t}})^2$. Figure 5 shows the variation of cross section as a function of coupling g_{ij}^{ut}, $(i,j=L \text{ or } R)$ for both cases (a) and (b) for different $M_{V_8^0}$ same as in the FC case.

We observe the growth of the cross section with the couplings due to the overall positive interference in Eq. (8) generated from large negative value of $\hat{t}$. It is also observed that the variations are comparatively

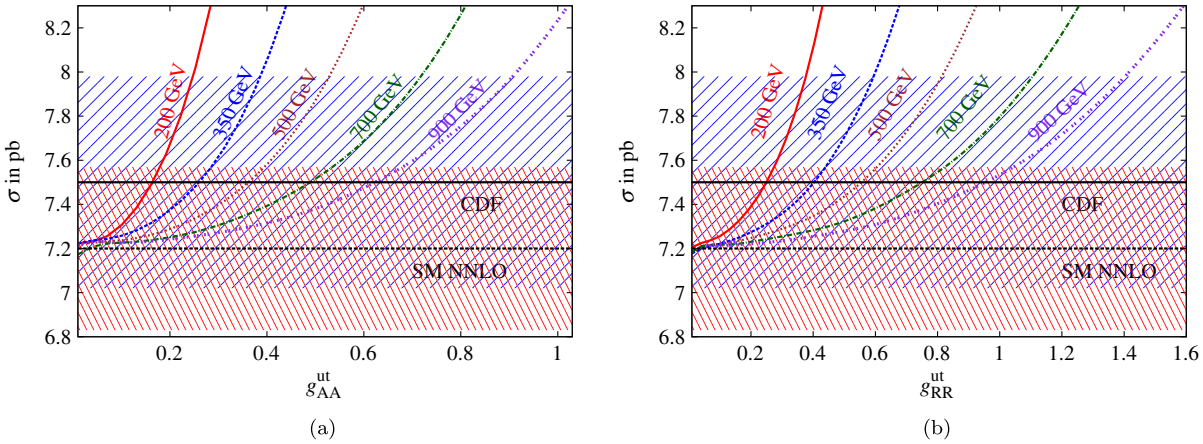

FIG. 5 (color online). Variation of the cross section $\sigma(p\bar{p}\to t\bar{t})$ with couplings g_{ij}^{ut} for flavor violating vector color octets corresponding to different values of $M_{V_8^0}$. The upper black dotted line associated with a blue band depicts the cross section 7.50 ± 0.48 pb from the CDF (all channels) [3], while the lower black dot-dashed line associated with a red band show theoretical estimate 7.2 ± 0.37 pb at NNLO [4]. (a) and (b) show the variation of σ for axial-vector and right-handed cases [the cases (a) and (b) of the text, respectively].

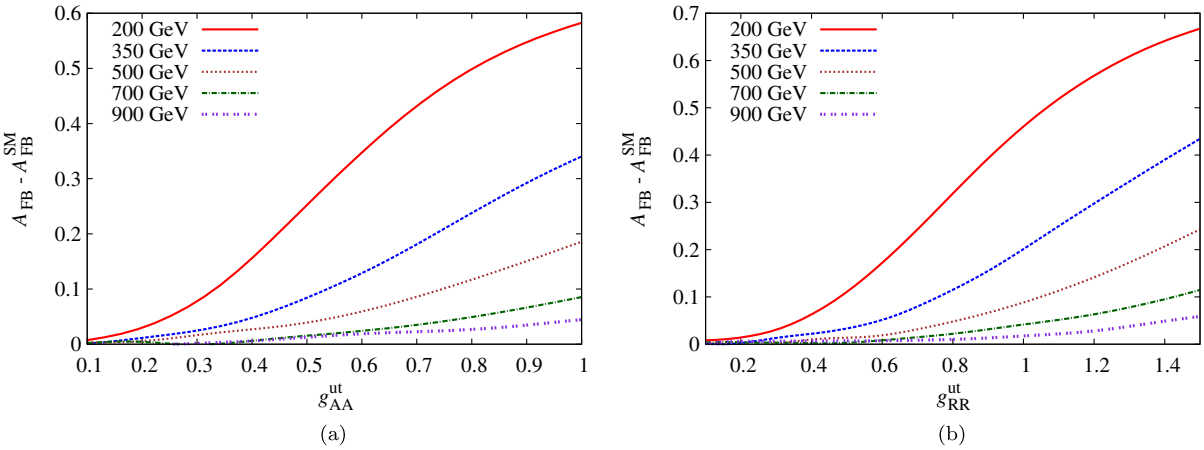

FIG. 6 (color online). Variation of the $A_{FB} - A_{FB}^{SM}$ with couplings g_{ij}^{ut} for flavor violating vector color octets corresponding to different values of $M_{V_8^0}$. (a) and (b) correspond to axial-vector and right-handed cases [the cases (a) and (b) of the text, respectively].

flat with respect to the corresponding cases of the flavor conserving scenarios due to the suppressed $\hat{t}$-channel propagator $(\hat{t} - m_{V_8}^2)^2 + \Gamma_{V_8^0}^2 M_{V_8^0}^2$ in the interference term.

A_{FB} as a function of couplings for both cases is plotted in Fig. 6. We find that A_{FB} is positive in both cases and increases with coupling, the increase being more rapid for lower mass.

The behavior of $C^{t\bar{t}}$ can be studied by writing the matrix element squared in terms of the same and opposite helicity contributions as before. From Eqs. (A3)–(A5), we define $\frac{d\hat{\sigma}_S^{FV}}{d\cos\theta}$ and $\frac{d\hat{\sigma}_O^{FV}}{d\cos\theta}$ as

$$\frac{d\hat{\sigma}_S^{FV}}{d\cos\theta} = g_s^4(1-\beta^2)\sin^2\theta\left[8 + \frac{2}{3}\frac{\hat{s}(\hat{t} - M_{V_8^0}^2)}{(\hat{t} - M_{V_8^0}^2)^2 + \Gamma_{V_8^0}^2 M_{V_8^0}^2}(g_L^{ut2} + g_R^{ut2}) + \frac{\hat{s}^2}{(\hat{t} - M_{V_8^0}^2)^2 + \Gamma_{V_8^0}^2 M_{V_8^0}^2}(g_L^{ut4} + g_R^{ut4})\right] + 8g_s^4 \frac{\hat{s}^2}{(\hat{t} - M_{V_8^0}^2)^2 + \Gamma_{V_8^0}^2 M_{V_8^0}^2} g_L^{ut2} g_R^{ut2}(1+\beta^2), \tag{9}$$

$$\frac{d\hat{\sigma}_O^{FV}}{d\cos\theta} = g_s^4(1+\cos^2\theta)\left[8 + \frac{2}{3}\frac{\hat{s}(\hat{t} - M_{V_8^0}^2)}{(\hat{t} - M_{V_8^0}^2)^2 + \Gamma_{V_8^0}^2 M_{V_8^0}^2}(g_L^{ut2} + g_R^{ut2}) + \frac{\hat{s}^2}{(\hat{t} - M_{V_8^0}^2)^2 + \Gamma_{V_8^0}^2 M_{V_8^0}^2}(g_L^{ut4} + g_R^{ut4})(1+\beta^2)\right] + g_s^4(2\beta\cos\theta)\left[\frac{2}{3}\frac{\hat{s}(\hat{t} - M_{V_8^0}^2)}{(\hat{t} - M_{V_8^0}^2)^2 + \Gamma_{V_8^0}^2 M_{V_8^0}^2}(g_L^{ut2} + g_R^{ut2}) + \frac{2\hat{s}^2}{(\hat{t} - M_{V_8^0}^2)^2 + \Gamma_{V_8^0}^2 M_{V_8^0}^2}(g_L^{ut4} + g_R^{ut4})\right]. \tag{10}$$

Analyzing the expression given in Eqs. (9) and (10) we find that the contribution of $\frac{d\hat{\sigma}_S^{FV}}{d\cos\theta}$ in vector/axial-vector case dominates over the $\frac{d\hat{\sigma}_O^{FV}}{d\cos\theta}$ due to the presence of the cross term proportional to $(g_L^{ut} g_R^{ut})^2$ and hence spin correlation decreases with the coupling as shown in the Fig. 7(a). In contrast, this cross term vanishes for the pure right-handed interactions and then the $\frac{d\hat{\sigma}_S^{FV}}{d\cos\theta}$ is suppressed by $(1-\beta^2)\sin^2\theta/(1+\beta^2)(1+\cos^2\theta)$ with respect to $\frac{d\hat{\sigma}_O^{FV}}{d\cos\theta}$, rendering $C^{t\bar{t}}$ to increase with the coupling as shown in Fig. 7(b).

Our results are in broad agreement with the existing results in the literature [31–34]. Their study was however based on the earlier results from the Tevatron [5] with the $A_{FB}^{t\bar{t}}$ dependence on $m_{t\bar{t}}$ in two regions of ≤ 450 GeV and ≥ 450 GeV, respectively.

C. χ^2 analysis

We have studied the production cross section and also the model contribution to the observables. We further analyze the one dimensional distribution plots and investigate the possibility to explain the observed $A_{FB}^{t\bar{t}}$ anomaly. Recently the CDF collaboration performed a detailed seven bin analysis with invariant mass distribution of $A_{FB}^{t\bar{t}}$ from the reconstructed top pairs [7]. They observed that the large forward-backward asymmetry comes from the higher

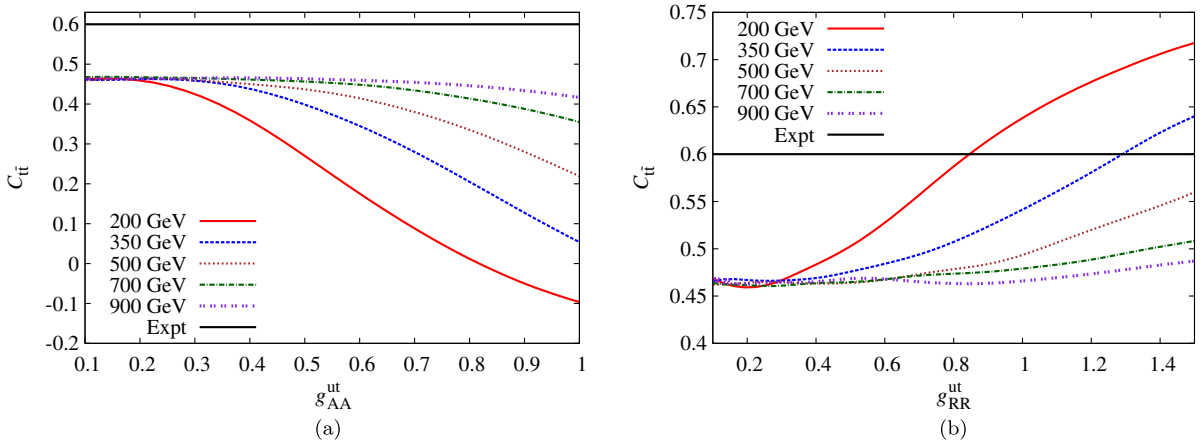

FIG. 7 (color online). Variation of the spin-correlation coefficient $C^{t\bar{t}}$ with couplings g^{ut}_{ij} for flavor violating vector color octets corresponding to different values of $M_{V_8^0}$. (a) and (b) correspond to axial-vector and right-handed cases [the cases (a) and (b) of the text, respectively].

invariant mass $M_{t\bar{t}}$ bins of the top-antitop pair. The forward-backward asymmetry as a function of $M_{t\bar{t}}$ is defined as

$$A_{\rm FB}(M_{t\bar{t}}) = \frac{N_F(M_{t\bar{t}}) - N_B(M_{t\bar{t}})}{N_F(M_{t\bar{t}}) + N_B(M_{t\bar{t}})}, \tag{11}$$

where N_F and N_B are the events in the forward and backward region, respectively. The analysis in Ref. [7] also gives the four bin analysis of the $A^{t\bar{t}}_{\rm FB}$ with the top-antitop rapidity difference distribution defined as

$$A_{\rm FB}(|\Delta y|) = \frac{N(\Delta y > 0) - N(\Delta y < 0)}{N(\Delta y > 0) + N(\Delta y < 0)}, \tag{12}$$

where rapidity difference $\Delta y = y_t - y_{\bar{t}}$, $N(\Delta y < 0)$ and $N(\Delta y > 0)$ are the number of events with positive and negative rapidity difference, respectively.

We scan our model parameter space for a given mass of the color-octet vector boson on the two dimensional plane of two distinct product of couplings which can provide the matched $m_{t\bar{t}}$ and Δy distribution of $A^{t\bar{t}}_{\rm FB}$ with the observed data. We perform χ^2 analysis for both FC and FV cases and predict the set of best parameters which can possibly explain the $A^{t\bar{t}}_{\rm FB}$ anomaly. To make this χ^2 study we take into account the $A^{t\bar{t}}_{\rm FB}$ distribution over $m_{t\bar{t}}$ bins as well as Δy bins from the full Run II Tevatron data set [7]. We define the combined χ^2 from the study of the $m_{t\bar{t}}$ and Δy distribution as For these analysis we use standard χ^2 fit, defined as

$$\chi^2 = \sum_i \frac{(\mathcal{O}_i^{\rm th} - \mathcal{O}_i^{\rm exp})^2}{(\delta\mathcal{O}_i)^2}, \tag{13}$$

where i is the $m_{t\bar{t}}$ or Δy bin index, and $\mathcal{O}_i$th and $\mathcal{O}_i^{\rm exp}$ are model and experimental estimate of the $A^{t\bar{t}}_{\rm FB}$ in the ith bin, respectively. The model estimate includes the both SM and new physics contribution. $\delta\mathcal{O}_i$ is the experimental error in the corresponding ith bin. We have considered seven and four suggested bins for the $m_{t\bar{t}}$ and Δy, respectively. In addition we have also considered the total cross section $\sigma(p\bar{p} \to t\bar{t}) = 7.5 \pm 0.31({\rm stat}) \pm 0.34({\rm syst}) \pm 0.15({\rm Ztheory})$ pb [2] as one of the observed data. Therefore we have used twelve observables to perform the analysis. For $\mathcal{O}_i$th we have taken the total cross section for this study as $\sigma^{\rm tot} = K \cdot \sigma^{\rm SM} + \sigma^{\rm NP}$, where $K = \frac{\sigma^{\rm NLO}}{\sigma^{\rm SM}} = 1.046$ and $A^{t\bar{t}}_{\rm FB} = A^{t\bar{t}}_{\rm FB}{}^{\rm SM\,NLO} + A^{t\bar{t}}_{\rm FB}{}^{\rm NP}$.

The two dimensional parameter space $[(\sqrt{\lambda_{LL}}, \sqrt{\lambda_{RR}})$ for FC cases and (g^{ut}_L, g^{ut}_R) for the FV case] with a given fixed mass is scanned leading to the minimum value of the $\chi^2 \equiv \chi^2_{\rm min}$. We plot histograms showing the $m_{t\bar{t}}$ spectrum of $A^{t\bar{t}}_{\rm FB}$ at combined $\chi^2_{\rm min}$ in Figs. 8(a), 8(c), and 8(e) for flavor conserving cases and Figs. 9(a), 9(c), and 9(e) for flavor violating cases, respectively. We have shown and compared the slope of our best-fit line with that from the experimental data in these figures and Tables II and IV. Similarly Figs. 8(b), 8(d), and 8(f) for flavor conserving cases and Figs. 9(b), 9(d), and 9(f) for flavor violating cases exhibit the Δy spectrum of $A^{t\bar{t}}_{\rm FB}$ at combined $\chi^2_{\rm min}$ along with the slope of the best fit line. These values for the Δy distribution of $A^{t\bar{t}}_{\rm FB}$ are also summarized in Tables III and V.

IV. SINGLE TOP

In the SM, a single top quark production is studied through three different channels with different final states, respectively, which have their own distinct kinematics and do not interfere with one another. The s-channel process takes place through an off-shell time like W boson which further decays into a top and bottom quark as shown in Fig. 10(a). The t-channel process is the dominant one and mediates through the exchange of a virtual W as shown in Fig. 10(c). The t-channel process resembles deep inelastic scattering while s-channel process resembles the Drell-Yan process. The single top quark production cross section in

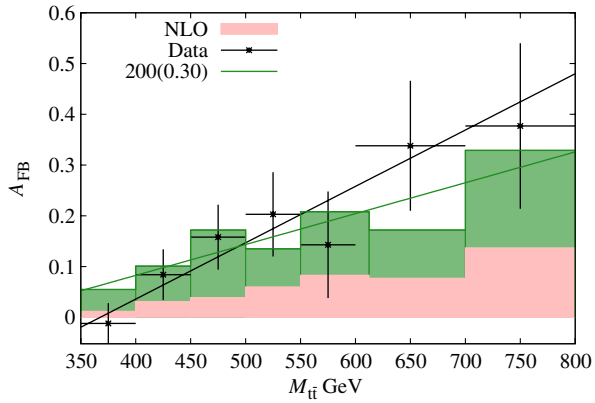

(a) $\lambda_{LL} = \lambda_{RR} = -\lambda_{RL} = -\lambda_{LR} = \lambda_{AA} = .30$

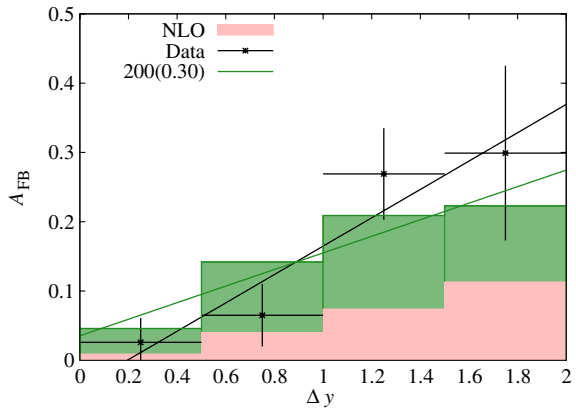

(b) $\lambda_{LL} = \lambda_{RR} = -\lambda_{RL} = -\lambda_{LR} = \lambda_{AA} = .30$

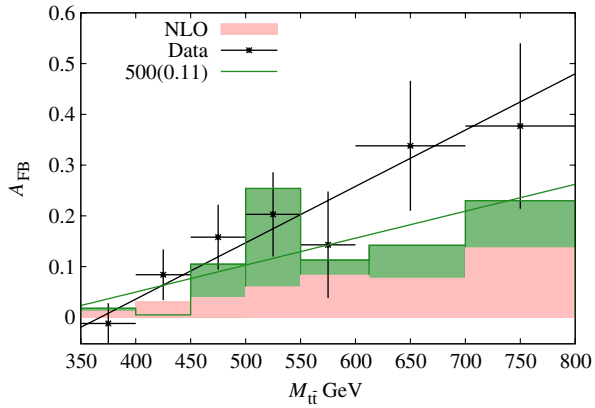

(c) $\lambda_{RR} = .11 \neq \lambda_{LR} = \lambda_{RL} = \lambda_{LL} = 0$

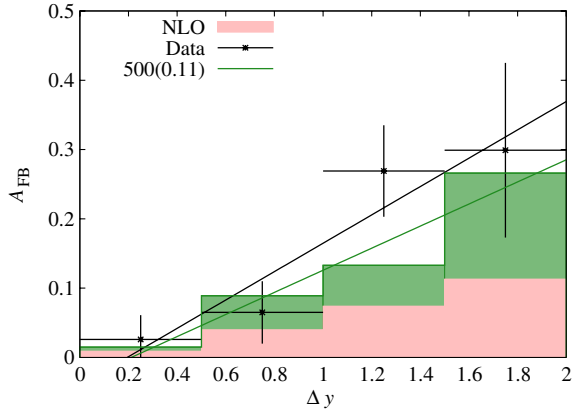

(d) $\lambda_{RR} = .11 \neq \lambda_{LR} = \lambda_{RL} = \lambda_{LL} = 0$

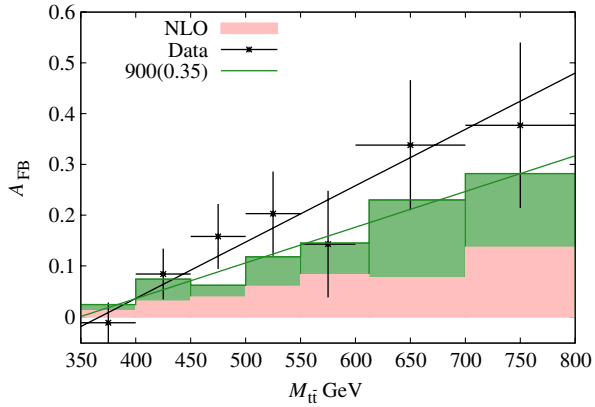

(e) $-\lambda_{LL} = -\lambda_{RR} = \lambda_{RL} = \lambda_{LR} = \lambda_{NA} = .35$

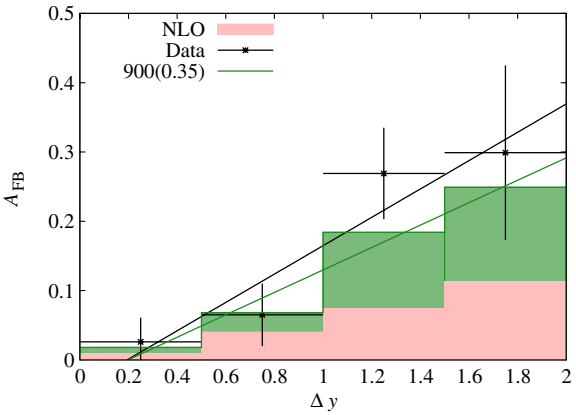

(f) $-\lambda_{LL} = -\lambda_{RR} = \lambda_{RL} = \lambda_{LR} = \lambda_{NA} = .35$

FIG. 8 (color online). $m_{t\bar{t}}$ and $|\Delta y|$ distribution of $A_{\mathrm{FB}}^{t\bar{t}}$ at χ^2_{min} for the three favorable point sets in parameter space at fixed $M_{V_8^0} = 200$, 500 and 900 GeV for flavor conserving case, shown in the shaded green histogram. The experimental data point is shown with its error in black, while the SM (NLO + QCD) with background subtracted are shown in the shaded pink histogram. The black line in all graphs is the best-fit line with the experimental data while the green line depicts the best-fit line with the model data.

these two modes have been estimated to be $\sigma^{\mathrm{NNNLO}}_{t\ \mathrm{channel}} = 1.05 \pm 0.11$ pb, $\sigma^{\mathrm{NNNLO}}_{s\ \mathrm{channel}} = 0.52 \pm 0.03$ pb, respectively, at the NNNLO approximation for $m_t = 173$ GeV [4]. Therefore the single top quark production in the t channel is roughly twice of the s-channel production cross section in the SM. The third channel for single top production is the associated tW production as shown in Fig. 10(b) which is estimated to be $\sigma^{\mathrm{NNNLO}}_{Wt\ \mathrm{channel}} = 0.11 \pm 0.04$ pb for $m_t = 173$ GeV [4]. We do not consider this process for our analysis. The single top quark production cross section in

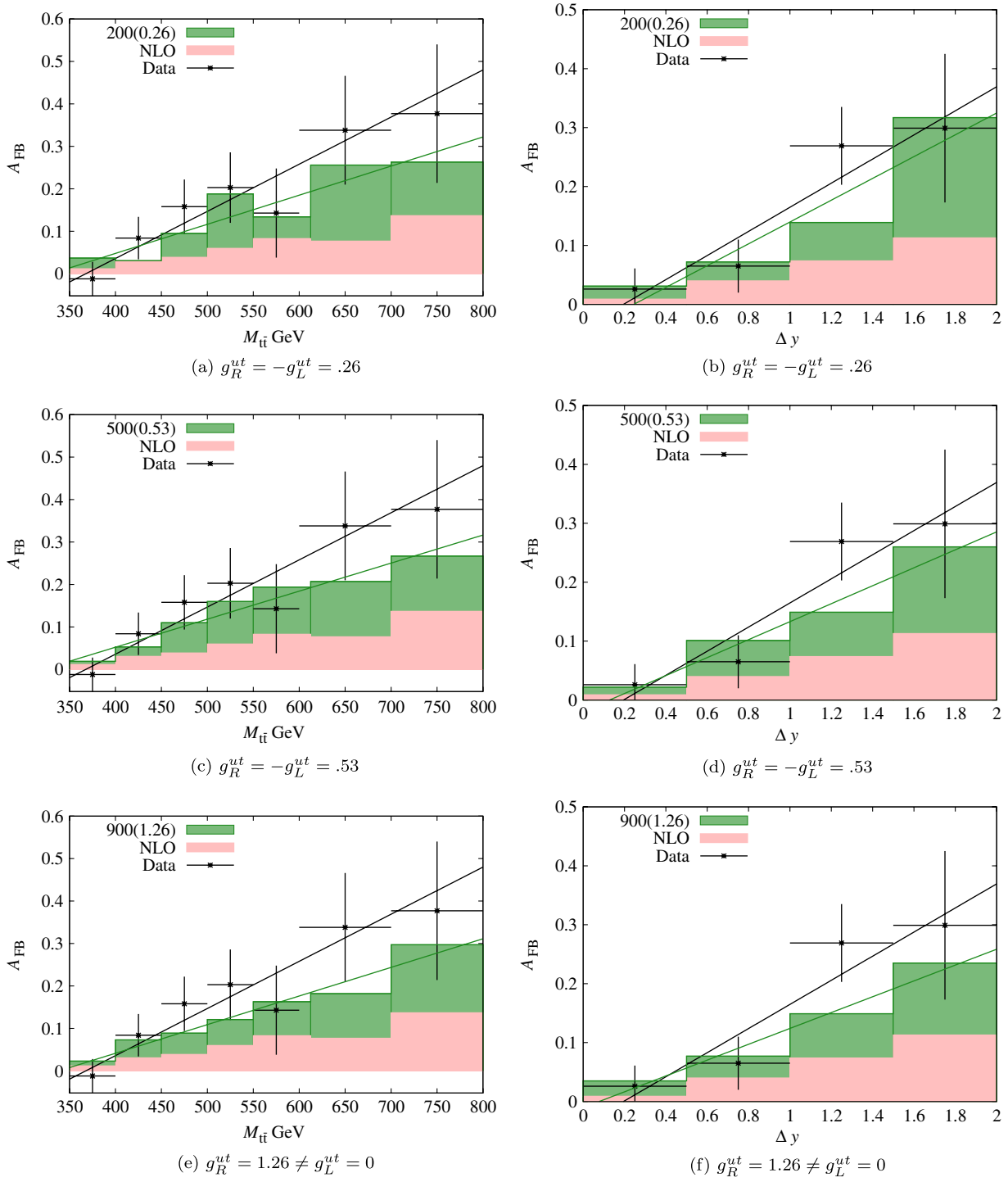

(a) $g_R^{ut} = -g_L^{ut} = .26$ (b) $g_R^{ut} = -g_L^{ut} = .26$

(c) $g_R^{ut} = -g_L^{ut} = .53$ (d) $g_R^{ut} = -g_L^{ut} = .53$

(e) $g_R^{ut} = 1.26 \neq g_L^{ut} = 0$ (f) $g_R^{ut} = 1.26 \neq g_L^{ut} = 0$

FIG. 9 (color online). $m_{t\bar{t}}$ and $|\Delta y|$ distribution of $A_{FB}^{t\bar{t}}$ at χ^2_{min} for the three favorable point sets in parameter space at fixed $M_{V_8^0} = 200$, 500 and 900 GeV for flavor violating case, shown in the shaded green histogram. The experimental data point is shown with its error in black, while the SM (NLO + QCD) with background subtracted are shown in the shaded pink histogram. The black line in all graphs is the best-fit line with the experimental data while the green line depicts the best-fit line with the model data.

the t channel is thus expected to dominate over the s-channel production both at the Tevatron and the LHC while the cross section for tW production is very small at the Tevatron but significant at the LHC. The three channels discussed above are sensitive to quite different manifestations of physics beyond the SM, such as FCNC, existence of color singlet/octet vector bosons $W'^{\pm}$, $H^{\pm}$, Z', $V_8^{\pm,0}$ etc., fourth generation quarks or detection of more general four

TABLE II. The first three columns give the bin limits of the $M_{t\bar{t}}$, the observed $A_{\rm FB}^{t\bar{t}}$ with error and the NLO (QCD + EW) generated $A_{\rm FB}^{t\bar{t}}$, respectively, [7]. The next three consecutive columns provide the differential $A_{\rm FB}^{t\bar{t}}$ corresponding to the model parameters [given in Figs. 8(a), 8(c), and 8(e)] leading to $\chi^2_{\rm min}$ at fixed coupling and $M_{V_8^0}$ in flavor conserving cases. The penultimate line gives the $\chi^2_{\rm min}$ for respective cases. The last line in the table gives the slope of the best fit line with the simulated data.

$M_{t\bar{t}}$	$A_{\rm FB}^{t\bar{t}}$ ($\pm$ stat)	NLO $t\bar{t}$-Bkg	200 GeV $\sqrt{\lambda_{AA}} = 0.30$	900 GeV $\sqrt{\lambda_{NAA}} = 0.35$	500 GeV $\sqrt{\lambda_{RR}} = 0.11$
$<$400 GeV	-0.012 ± 0.040	0.012	0.055	0.024	0.018
400–450 GeV	0.084 ± 0.050	0.031	0.101	0.074	0.005
450–500 GeV	0.158 ± 0.064	0.039	0.172	0.062	0.105
500–550 GeV	0.203 ± 0.083	0.060	0.135	0.118	0.254
550–600 GeV	0.143 ± 0.105	0.083	0.208	0.145	0.113
600–700 GeV	0.338 ± 0.128	0.077	0.172	0.230	0.142
$\geq$ 700 GeV	0.377 ± 0.163	0.137	0.329	0.282	0.230
$\chi^2_{\rm min}$	...	...	6.05	5.27	7.43
Slope of best-fit line	$(11.1 \pm 2.9) \times 10^{-4}$	3.0×10^{-4}	6.08×10^{-4}	7.04×10^{-4}	5.31×10^{-4}

TABLE III. The first three columns give the bin limits of the $|\Delta y|$, the observed $A_{\rm FB}^{t\bar{t}}$ with error and the NLO (QCD + EW) generated $A_{\rm FB}^{t\bar{t}}$, respectively, [7]. The next three consecutive columns provide the differential $A_{\rm FB}^{t\bar{t}}$ corresponding to the model parameters [given in Figs. 8(b), 8(d), and 8(f)] leading to $\chi^2_{\rm min}$ at fixed coupling and $M_{V_8^0}$ in flavor conserving cases. The penultimate line gives the $\chi^2_{\rm min}$ for respective cases. The last line in the table gives the slope of the best fit line with the simulated data.

$\lvert\Delta y\rvert$	$A_{\rm FB}^{t\bar{t}}$ ($\pm$ stat)	NLO $t\bar{t}$-Bkg	200 GeV $\sqrt{\lambda_{AA}} = 0.30$	900 GeV $\sqrt{\lambda_{NAA}} = 0.35$	500 GeV $\sqrt{\lambda_{RR}} = 0.11$
0.0–0.5	0.026 ± 0.035	0.009	0.046	0.018	0.015
0.5–1.0	0.065 ± 0.045	0.040	0.142	0.068	0.089
1.0–1.5	0.269 ± 0.066	0.074	0.209	0.184	0.133
$\geq$ 1.5	0.299 ± 0.126	0.113	0.223	0.249	0.266
$\chi^2_{\rm min}$	...	...	4.41	1.87	4.73
Slope of best-fit line	$(20.0 \pm 5.9) \times 10^{-2}$	6.7×10^{-2}	11.96×10^{-2}	16.18×10^{-2}	15.94×10^{-2}

TABLE IV. Same as Table I; first column gives the bin limits of the $M_{t\bar{t}}$ and the next three consecutive columns provide the differential $A_{\rm FB}^{t\bar{t}}$ corresponding to the model parameters [given in Figs. 9(a), 9(c), and 9(e)] leading to $\chi^2_{\rm min}$ in flavor violating cases.

$M_{t\bar{t}}$	200 GeV $g_{AA}^{ut} = 0.26$	500 GeV $g_{AA}^{ut} = 0.53$	900 GeV $g_{RR}^{ut} = 1.26$
$<$400 GeV	0.037	0.019	0.023
400–450 GeV	0.031	0.053	0.073
450–500 GeV	0.095	0.110	0.089
500–550 GeV	0.188	0.160	0.121
550–600 GeV	0.134	0.194	0.163
600–700 GeV	0.256	0.207	0.182
$\geq$ 700 GeV	0.263	0.267	0.297
$\chi^2_{\rm min}$	4.92	4.14	4.93
Slope of best-fit line	6.85×10^{-4}	6.6×10^{-4}	6.74×10^{-4}

TABLE V. Same as Table II; first column gives the bin limits of the $|\Delta y|$ and the next three consecutive columns provide the differential $A_{\rm FB}^{t\bar{t}}$ corresponding to the model parameters [given in Figs. 9(b), 9(d), and 9(f)] leading to $\chi^2_{\rm min}$ in flavor violating cases.

$\lvert\Delta y\rvert$	200 GeV $g_{AA}^{ut} = 0.26$	500 GeV $g_{AA}^{ut} = 0.53$	900 GeV $g_{RR}^{ut} = 1.26$
0.0–0.5	0.031	0.022	0.035
0.5–1.0	0.072	0.101	0.077
1.0–1.5	0.139	0.149	0.149
≥ 1.5	0.317	0.260	0.235
$\chi^2_{\rm min}$	3.97	4.03	3.71
Slope of best-fit line	18.5×10^{-2}	15.24×10^{-2}	13.44×10^{-2}

fermion interactions. D0 reported the s-channel and t-channel cross sections to be $\sigma_s = 0.68^{+0.38}_{-0.35}$ pb and $\sigma_t = 2.86^{+0.69}_{-0.63}$ pb for $m_t = 172.5\,\text{GeV}$, respectively, [14] in agreement with the estimated cross sections in the SM. However, very recently the CDF collaboration [13] using 7.5 fb^{-1} of $p\bar{p}$ collisions data collected in the Run II experiment obtained $\sigma_s = 1.81^{+0.63}_{-0.58}$ pb and $\sigma_t = 1.49^{+0.47}_{-0.42}$ pb where in the central values of s- and t-channel cross sections are comparable. This is in conflict with the SM NNNLO prediction. The total single top cross section measured by this group $\sigma_{\rm total} = 3.04^{+0.57}_{-0.53}$ pb for $m_t = 172.5$ GeV is however consistent with the total single top production in the SM at the NNNLO approximation.

There are two alternative approaches available in the literature to study t-channel single top quark production at the LO and NLO. One of the approaches is based on the $2 \to 2$ scattering process Fig. 10(c), where b quark is taken to be present in the initial state. This is so called five flavor (5F) scheme. In this scheme the presence of b jet and the effect of b mass appears only at the NLO. In the second approach the LO (Born process) is the $2 \to 3$ scattering process Fig. 10(d). In this four flavor (4F) scheme, the b quark does not enter in the QCD evolution of the parton distribution function. For details see [50,51]. The approaches are shown to be equivalent and give the same result at all orders in the perturbation expansion. In the present work we treat the proton in the 5F scheme and study the b-initiated $2 \to 2$ process since we are only interested in estimation of the total production cross section [52].

In this section we will study single top s-channel and t-channel production in $\mathbf{3} \otimes \bar{\mathbf{3}}$ model in flavor conserving and flavor violating cases. Throughout our analysis we assume $|V_{tb}| = 1$. In the flavor conserving case, the single top production in the s channel and t channel proceeds through the charge current interactions through $V_8^{\pm}$ as shown in Figs. 11(a) and 11(b), respectively. The flavor violating mode mediates through flavor changing neutral current via V_8^0 as shown in Figs. 11(c) and 11(d), respectively. The charged octet vector boson does not contribute to the other processes in the top quark sector addressed in our study. However, the contribution of the FCNC is likely to provide the common global allowed parameter space of the model from all the processes involving the top quark sector.

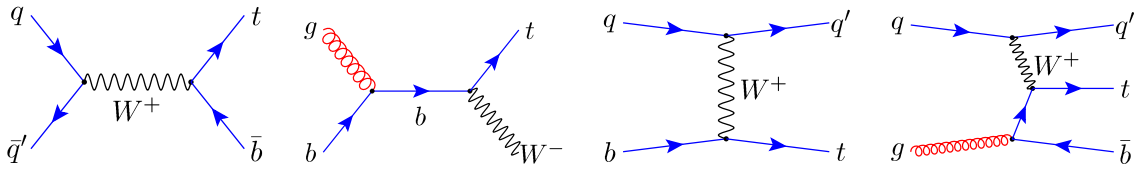

(a) s-channel (b) Wt- channel (c) $2 \to 2$ t-channel (d) $2 \to 3$ t-channel

FIG. 10 (color online). Leading order single top production channels in SM.

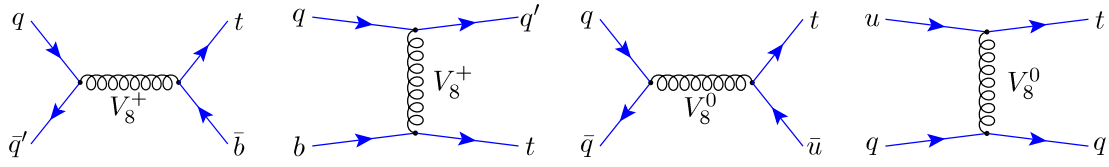

(a) s-channel CC (b) t-channel CC (c) s-channel NC (d) t-channel NC

FIG. 11 (color online). Leading order single top production channels mediated by the charged color-octet vector current are shown in (a) and (b), and the flavor violating neutral color-octet vector current is shown in (d) and (e), respectively.

A. Flavor conserving

The differential cross sections with respect to the emerging angle of the single massive top quark $\cos\theta_t$ the s-channel subprocess $u\bar{d} \to t\bar{b}$, and the t-channel subprocess $ub \to td$ are given as

$$\frac{d\sigma_{u\bar{d}\to t\bar{b}}}{d\cos\theta_t} = \frac{\pi\beta'\alpha_s^2}{18\hat{s}} \frac{1}{(\hat{s}-M_{V_8}^2)^2 + M_{V_8}^2\Gamma_{V_8}^2} \times [\mathcal{C}_+\hat{u}(\hat{u}-m_t^2) + \mathcal{C}_-\hat{t}(\hat{t}-m_t^2)], \quad (14)$$

$$\frac{d\sigma_{ub\to td}}{d\cos\theta_t} = \frac{\pi\beta'\alpha_s^2}{18\hat{s}} \frac{1}{(\hat{t}-M_{V_8}^2)^2 + M_{V_8}^2\Gamma_{V_8}^2} \times [\mathcal{C}_+\hat{s}(\hat{s}-m_t^2) + \mathcal{C}_-\hat{t}(\hat{t}-m_t^2)], \quad (15)$$

where

$$\mathcal{C}_\pm = (|C_L^{tb}|^2 + |C_R^{tb}|^2)(|C_L^{ud}|^2 + |C_R^{ud}|^2) \pm (|C_L^{tb}|^2 - |C_R^{tb}|^2)(|C_L^{ud}|^2 - |C_R^{ud}|^2)$$
$$\text{and} \quad \beta' = 1 - \frac{m_t^2}{\hat{s}}. \quad (16)$$

It is evident from Eq. (16) that the contribution for the pure vector current and pure axial current is identical which also holds true between the right and left chiral contributions. We study the variation of the single top quark production in the s channel with the couplings for various vector octet masses which are shown in Figs. 12(a) and 12(b) corresponding to the charged axial and right-chiral current, respectively. We observe the sharp growth in the cross sections even with the smaller couplings and later flattens out with the increasing mass of the octet.

Figures 12(c) and 12(d) depict the variation in the t-channel mode. It is evident that the plugging of decay

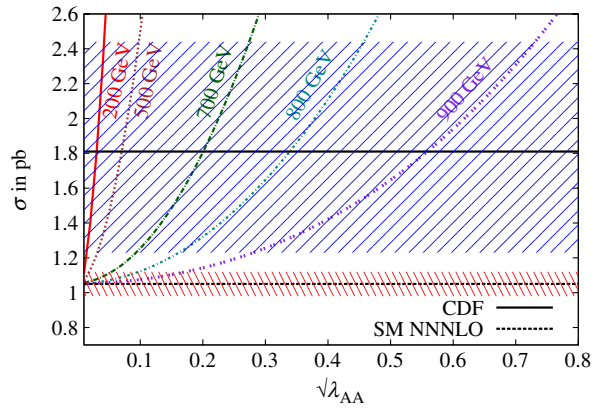

(a) s channel $\sigma(p\bar{p} \to t\bar{b} + \bar{t}b)$: $\lambda_{LL} = \lambda_{RR} = -\lambda_{RL} = -\lambda_{LR} = \lambda_{AA}$

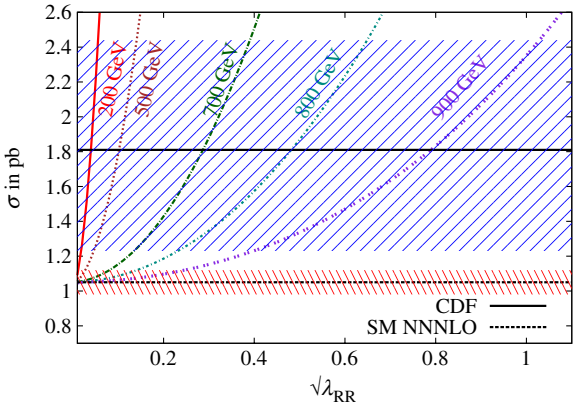

(b) s channel $\sigma(p\bar{p} \to t\bar{b} + \bar{t}b)$: $\lambda_{RR} \neq 0 = \lambda_{LR} = \lambda_{RL} = \lambda_{LL}$

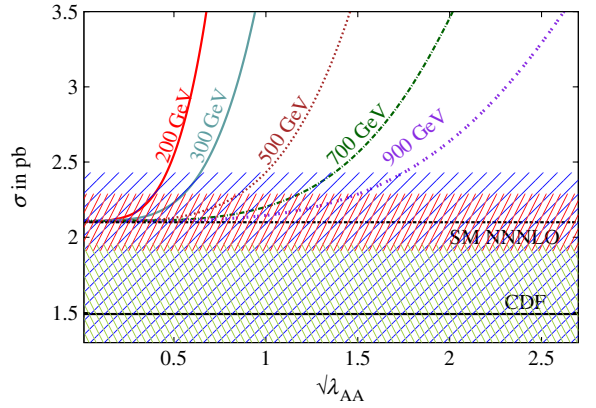

(c) t channel $\sigma(p\bar{p} \to tj + \bar{t}j)$: $\lambda_{LL} = \lambda_{RR} = -\lambda_{RL} = -\lambda_{LR} = \lambda_{AA}$

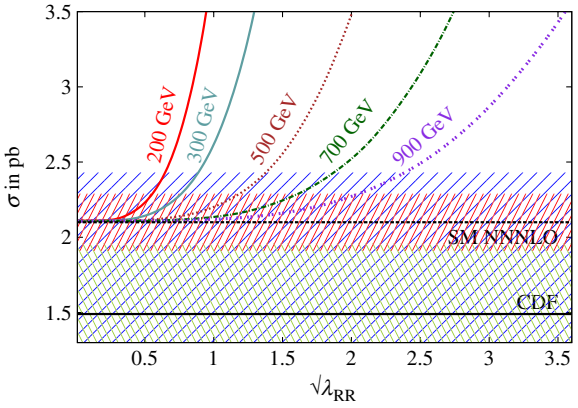

(d) t channel $\sigma(p\bar{p} \to tj + \bar{t}j)$: $\lambda_{RR} \neq 0 = \lambda_{LR} = \lambda_{RL} = \lambda_{LL}$

FIG. 12 (color online). Variation of the cross section with flavor conserving couplings for various vector color-octet masses $M_{V_8^\pm}$. In the top panels in (a) and (b) the upper dotted black line and associated blue band depict the CDF central value and the one sigma band, respectively, for s-channel cross section $1.81^{+0.63}_{-0.58}$ pb [13], while the lower dot-dashed black line with a red band shows the theoretical central value and the one sigma band, respectively, for 1.05 ± 0.07 pb at NNNLO [4]. Similarly in the lower panels (c) and (d) the experimental central value is shown with the lower dotted black line and the associated 1-sigma green band and 2-sigma blue band correspond to t-channel cross section $1.49^{+0.47}_{-0.42}$ pb from CDF [13]. The upper dot-dashed black line associated with a red band shows the theoretical central value and one sigma band for 2.10 ± 0.19 pb at NNNLO [4].

width in the t-channel propagator flattens the variation of the curve with respect to couplings. Since there is no interference between the SM and color-octet model (for both the channels), we find that the cross section grows with the coupling and decreases with the mass of the color-octet vector bosons.

B. Flavor violating

FCNC induces additional channels for single top quark production. These additional Feynman diagrams are shown in Figs. 11(c) and 11(d). This contribution is realized through the flavor changing coupling $g^{ut}_{L,R}$ at one of the vertices only but can be mediated through both s and t channels. This then would make the life uncomfortable for measuring s and t channels separately as the final states for both the diagrams are the same. For this we need to have a combined study of s and t channels with one FV vertex from the new physics sector. Thus the new physics contribution at the amplitude level is proportional to the product of the flavor conserving coupling $g^{q}_{L,R}$ and flavor violating coupling $g^{ut}_{L,R}$. We define $\sqrt{f^{q,ut}_{ij}} = \sqrt{g^{q}_{i} g^{ut}_{j}}$ for $i \equiv L, R, V, A$. The differential cross section with respect to $\cos\theta_t$ for the s-channel subprocess $q\bar{q} \to t\bar{u}(q = d, s, c, b)$, $s + t$ channel subprocess $u\bar{u} \to t\bar{u}$ and $t + u$ channel subprocess $uu \to tu$ assuming top quark mass m_t and others to be massless is given as

$$\frac{d\sigma_{q\bar{q}\to t\bar{u}}}{d\cos\theta_t} = \frac{\pi\beta'\alpha_s^2}{18\hat{s}} \frac{1}{(\hat{s} - M^2_{V^0_8})^2 + M^2_{V_8}\Gamma^2_{V^0_8}} [\mathcal{V}_+ \hat{u}(\hat{u} - m_t^2) + \mathcal{V}_- \hat{t}(\hat{t} - m_t^2)] \tag{17}$$

$$\begin{aligned}\frac{d\sigma_{u\bar{u}\to t\bar{u}}}{d\cos\theta_t} = \frac{\pi\beta'\alpha_s^2}{18\hat{s}} \Bigg\{ & \frac{1}{(\hat{s} - M^2_{V^0_8})^2 + M^2_{V^0_8}\Gamma^2_{V^0_8}} [\mathcal{V}_+ \hat{u}(\hat{u} - m_t^2) + \mathcal{V}_- \hat{t}(\hat{t} - m_t^2)] \\ & - \frac{2}{3} \frac{(\hat{s} - M^2_{V^0_8})}{(\hat{s} - M^2_{V^0_8})^2 + M^2_{V^0_8}\Gamma^2_{V^0_8}} \frac{(\hat{t} - M^2_{V^0_8})}{(\hat{t} - M^2_{V^0_8})^2 + M^2_{V^0_8}\Gamma^2_{V^0_8}} \hat{u}(\hat{u} - m_t^2)[(g^{uu}_L g^{ut}_L)^2 + g^{uu}_R g^{ut}_R)^2] \\ & + \frac{1}{(\hat{t} - M^2_{V^0_8})^2 + M^2_{V^0_8}\Gamma^2_{V^0_8}} [\mathcal{V}_+ \hat{s}(\hat{s} - m_t^2) + \mathcal{V}_- \hat{u}(\hat{u} - m_t^2)] \Bigg\},\end{aligned} \tag{18}$$

$$\begin{aligned}\frac{d\sigma_{uu\to tu}}{d\cos\theta_t} = \frac{\pi\beta'\alpha_s^2}{18\hat{s}} \Bigg\{ & \frac{1}{(\hat{t} - M^2_{V^0_8})^2 + M^2_{V^0_8}\Gamma^2_{V^0_8}} [\mathcal{V}_+ \hat{u}(\hat{u} - m_t^2) + \mathcal{V}_- \hat{s}(\hat{s} - m_t^2)] \\ & + \frac{2(\hat{t} - M^2_{V^0_8})(\hat{u} - M^2_{V^0_8})}{((\hat{t} - M^2_{V^0_8})^2 + M^2_{V^0_8}\Gamma^2_{V^0_8})((\hat{u} - M^2_{V^0_8})^2 + M^2_{V^0_8}\Gamma^2_{V^0_8})} \hat{s}(\hat{s} - m_t^2)[(g^{uu}_L g^{ut}_L)^2 + g^{uu}_R g^{ut}_R)^2] \\ & + \frac{1}{(\hat{u} - M^2_{V^0_8})^2 + M^2_{V^0_8}\Gamma^2_{V^0_8}} [\mathcal{V}_+ \hat{t}(\hat{t} - m_t^2) + \mathcal{V}_- \hat{s}(\hat{s} - m_t^2)] \Bigg\},\end{aligned} \tag{19}$$

where

$$\mathcal{V}_\pm = (|g^{ut}_L|^2 + |g^{ut}_R|^2)(|g^{qq}_L|^2 + |g^{qq}_R|^2) \pm (|g^{ut}_L|^2 - |g^{ut}_R|^2)(|g^{qq}_L|^2 - |g^{qq}_R|^2).$$

Since the amplitude is the quadratic symmetric function of the left and right-handed couplings, the axial and vector currents are identical and so is the case for right- and left-handed currents. We have also taken into account the additional decay channels contributing to the total decay width of the color-octet neutral vector boson due to the introduction of FV couplings. We exhibit the variation of the single top quark production with the product of the couplings $\sqrt{f^{q,ut}_{ij}}$ for different flavor violating color-octet neutral vector boson masses in Figs. 13(a) and 13(b) corresponding to the axial and right-chiral currents. We observe that the couplings f_i are quite sensitive to the production cross section for the cases. It would then imply

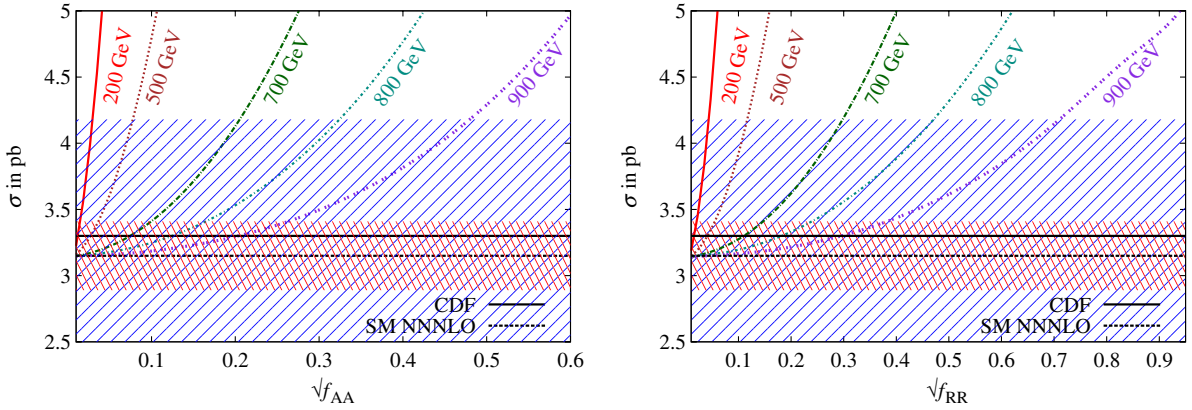

(a) $f_{LL}^{q,ut} = f_{RR}^{q,ut} = -f_{RL}^{q,ut} = -f_{LR}^{q,ut} = f_{AA}^{q,ut}$ (b) $f_{RR}^{q,ut} \neq 0 = f_{LR}^{q,ut} = f_{RL}^{q,ut} = f_{LL}^{q,ut}$

FIG. 13 (color online). Variation of the combined cross section $\sigma(p\bar{p} \to t\bar{b} + \bar{t}b)$ and $\sigma(p\bar{p} \to tj + \bar{t}j)$ with couplings $\sqrt{f_{ij}^{q,ut}}$ corresponding to different values of $M_{V_8^0}$. In (a) and (b) the upper dotted black line and associated blue band depict the central value of combined experimental $s + t$ channel cross section and one sigma allowed region of $3.04^{+0.57}_{-0.53}$ pb from the CDF [13], while the lower dot-dashed black line with a red band shows the theoretical estimate and its uncertainty 3.15 ± 0.26 pb at NNNLO [4].

that for a given FC coupling the single top production can constrain the FV coupling more severely than the top-pair production.

V. SAME-SIGN TOP

Introduction of the flavor violating couplings involving first and third generation for the top-pair production also induces the new channel for same-sign top/antitop pair production. The same-sign top production is highly suppressed in SM because it involves higher order flavor changing neutral current interactions.

In the present study the process $uu(\bar{u}\,\bar{u}) \to tt(\bar{t}\,\bar{t})$ proceeds through the exchange of neutral color-octet vector boson V_8^0 with flavor changing neutral current interactions between the first and third generation only in the t channel and the exchange diagram u channel as shown in Fig. 14.

The differential cross section for $uu(\bar{u}\,\bar{u}) \to tt(\bar{t}\,\bar{t})$ with respect to the cosine of the top quark polar angle θ in the tt c.m. frame is

$$\frac{d\hat{\sigma}}{dcos\theta} = \frac{\pi\beta\alpha_s^2}{(\hat{t} - M_{V_8^0}^2)^2 + M_{V_8^0}^2\Gamma_{V_8^0}^2}\frac{\hat{s}}{18}[2(g_L^{ut4} + g_R^{ut4}) + g_L^{ut2}g_R^{ut2}(1 + \beta cos\theta)^2]$$
$$+ \frac{2\pi\beta\alpha_s^2(\hat{t} - m_{V_8^0}^2)(\hat{u} - m_{V_8^0}^2)}{((\hat{t} - M_{V_8^0}^2)^2 + M_{V_8^0}^2\Gamma_{V_8^0}^2)((\hat{u} - M_{V_8^0}^2)^2 + M_{V_8^0}^2\Gamma_{V_8^0}^2)}\frac{\hat{s}}{9}\left[(g_L^{ut4} + g_R^{ut4}) - 2g_L^{ut2}g_R^{ut2}\frac{m_t^2}{\hat{s}}\right]$$
$$+ \frac{\pi\beta\alpha_s^2}{(\hat{u} - M_{V_8^0}^2)^2 + M_{V_8^0}^2\Gamma_{V_8^0}^2}\frac{\hat{s}}{18}[2(g_L^{ut4} + g_R^{ut4}) + g_L^{ut2}g_R^{ut2}(1 - \beta cos\theta)^2], \quad (20)$$

where $\hat{s} = (p_u + p_u)^2$ is the squared c.m. energy of the system with top quark velocity $\beta = \sqrt{1 - 4m_t^2/\hat{s}}$.

We study the variation of the production cross section $\sigma(p\bar{p} \to tt + \bar{t}\,\bar{t})$ with respect to axial-vector and right-chiral FCNC couplings, respectively. To compare with the experimental results we allow these tops/antitops to decay through leptonic channels only as shown in Figs. 15(a) and 15(b). However, the nonobservability of same-sign dilepton events at the hadronic colliders restricts the parameter space of the model generating such events. In Fig. 16(a) we depict the constrain on the left- and right-chiral couplings from the observed cross section of $\sigma(p\bar{p} \to tt + \bar{t}\,\bar{t}) \times \mathrm{BR}[W \to l\nu]^2 \leq 0.54$ pb for the combined signature of the same-sign top-pair and same-sign antitop pair production and then decaying through the respective leptonic channels [16]. CMS [17] and ATLAS [18] data constrain the parameter space from $\sigma(pp \to tt)$ only with observed cross section ≤ 17 pb and ≤ 1.7 pb, respectively. Figures 16(b) and 16(c) provide the

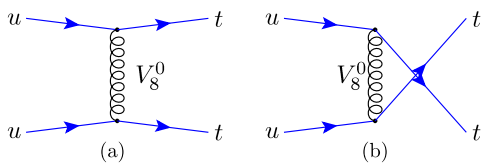

FIG. 14 (color online). Diagrams for same-sign top production through V_8^0 in (a) t and (b) u channels.

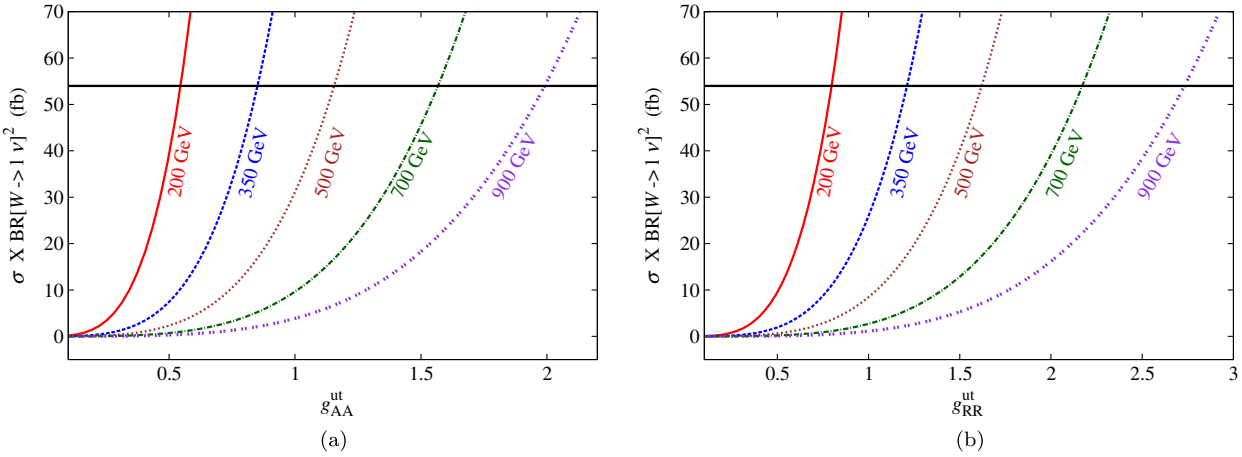

FIG. 15 (color online). Variation of the cross section $\sigma(p\bar{p} \to tt + \bar{t}\,\bar{t})$ times branching ratio (BR) $\mathrm{BR}(W \to l\nu)^2$ with couplings g^{ut}_{ij} for flavor violating vector color octets corresponding to different values of $M_{V_8^0}$ GeV for both the cases (a) and (b) given in the text. The upper dotted line depicts the maximum allowed $\sigma_{tt+\bar{t}\,\bar{t}} \times \mathrm{BR}(W \to l\nu)^2 = 54$ fb with a 95% confidence level [16].

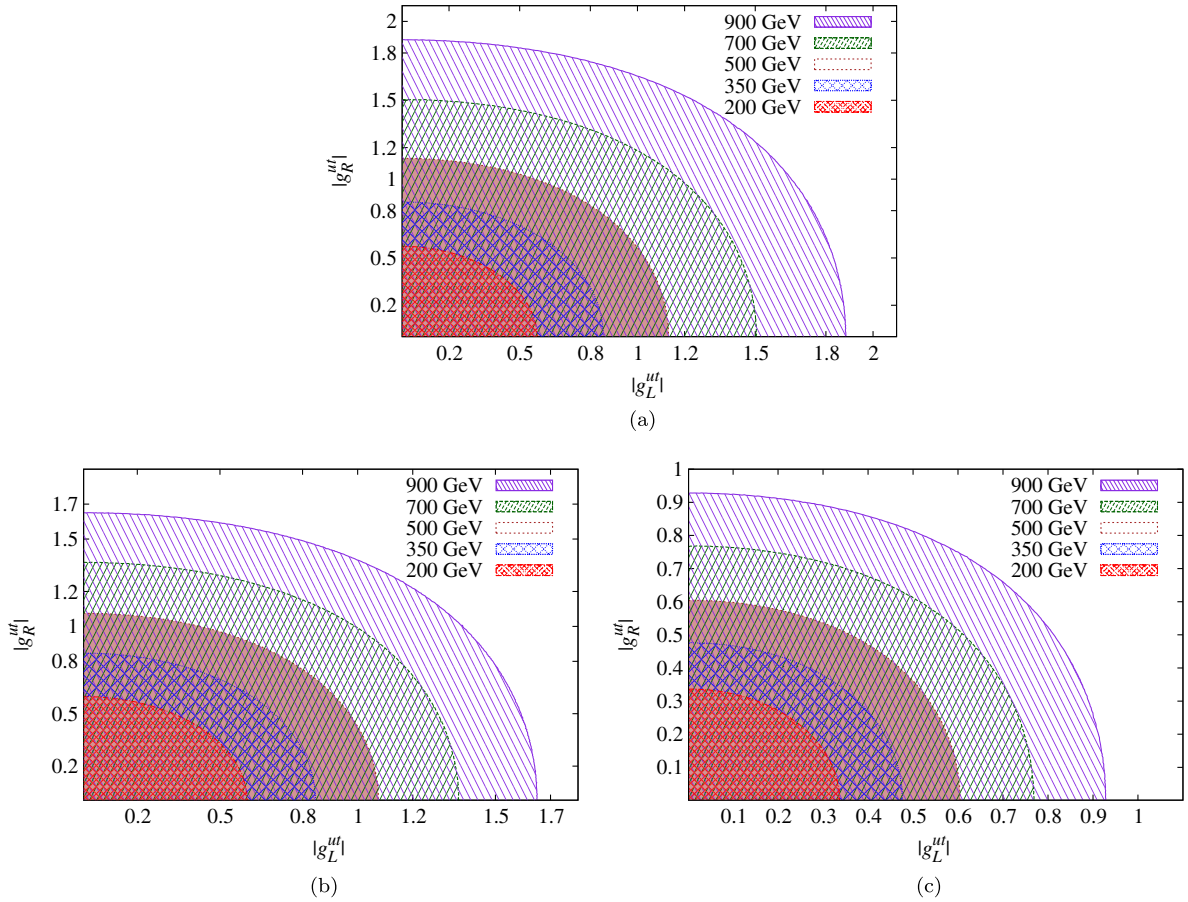

FIG. 16 (color online). 95% CL exclusion contours on the plane of g^{ut}_L and g^{ut}_R for varying color-octet masses. (a) corresponds to $\sigma(p\bar{p} \to tt + \bar{t}\,\bar{t}) \times \mathrm{BR}[W \to l\nu]^2 \leq 54$ fb from Tevatron at the CDF [16]. (b) corresponds to measurement from CMS at the LHC, constraining $\sigma(pp \to tt(j)) \leq 17$ pb [17] and (c) corresponds to $\sigma(pp \to tt) \leq 1.7$ pb from the ATLAS detector at the LHC [18].

95% confidence level exclusion contours in the two dimensional plane of flavor violating chiral couplings g_L^{ut} and g_R^{ut} for a given color-octet mass corresponding to the observed data from CMS and ATLAS, respectively.

We observe that these contours severely narrows the allowed parameter space contributing to the top-antitop pair production and generating the positive $A_{\rm FB}^{t\bar{t}}$.

VI. CONSISTENCY WITH THE $t\bar{t}$ AND DIJET PRODUCTION AT LHC

In the previous section we investigated the parameter region for color-octet vector bosons and found constraints on the masses and couplings by taking total top quark pair production at the Tevatron including single top quark production and same-sign top quark production cross sections. We then analyzed the exclusion region of the parameters via same-sign top quark pair production at the Tevatron as well as at the LHC. Additionally, fitted data for $A_{\rm FB}^{t\bar{t}}$ at the Tevatron restricted the parameter space further and gave some favorable parameters in the model considered in this article. Further investigations can then lead to exclusion/acceptance of the parameters by studying transverse momentum of the final states and invariant mass differential distributions for top-pair and dijet production cross sections. The other observables like S, T parameters and the Z decay width effects further constraint the color-octet vector boson model but these studies are beyond the scope of this article; detailed studies can be found in [39]. In this section we investigate the consistency of the favorable parameters found at the Tevatron by studying the cross section, charge asymmetry, spin correlation, invariant mass differential distributions for top quark pair production and dijets production data at the LHC.

A. $t\bar{t}$ production and $m_{t\bar{t}}$ distribution

The color-octet vector bosons not only contribute to the $t\bar{t}$ production cross section both at the Tevatron and the LHC but modify its shape as a function of invariant mass $m_{t\bar{t}}$ as well. The $t\bar{t}$ resonance searches will put constraints on the resonance mass. For $t\bar{t}$ production, the decay width of the color-octet vector boson is relevant for $M_{V_8} > 2m_t$ so that the top pair can be produced at resonance. Earlier studies incorporated rather large values of the decay width, e.g., $\Gamma_{V_8} \approx 0.1$–$0.2 M_{V_8}$. We have on the other hand used the width calculated for the parameters employed in our study of the cross sections.

We explore the subspace of the parameters of the color octets which can explain the observed forward-backward asymmetry at the Tevatron as discussed in Sec. III C and thus attempt to examine the admissibility of these data points with respect to the recently observed LHC data. As a first step, we compare the cross section of the Tevatron and the LHC for the $t\bar{t}$ production corresponding to the same values of the couplings with a given resonant mass and the nature of the exchange current. This is shown in Fig. 17(a) where the $t\bar{t}$ cross section induced by the flavor conserving couplings within the allowed experimental limits for the Tevatron and the LHC are depicted on the x and y axes, respectively. To highlight the chosen data points we mark the focus points in the figure along with a prediction from the SM. The two vertical lines in the figure corresponds to the 1-σ boundaries of the maximum allowed $\sigma_{t\bar{t}}$ at the Tevatron [2,3]. It is clear from the figure that the observed $\sigma_{t\bar{t}}$ at the Tevatron completely lies within the experimentally observed range of $\sigma_{t\bar{t}}$ at the LHC [53]. In Fig. 17(b) the same is plotted for the flavor violation case.

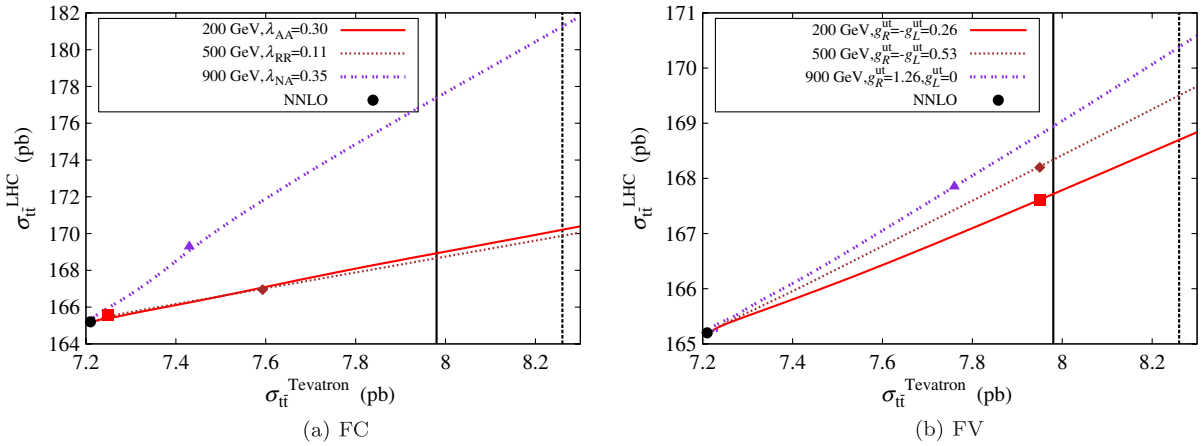

(a) FC (b) FV

FIG. 17 (color online). The x and y coordinates on the curve depict the production cross sections $\sigma_{t\bar{t}}$ at the Tevatron and the LHC, respectively, corresponding to a fixed value of the coupling and the resonant mass for (a) flavor conserving and (b) flavor violating cases. The highlighted colored data points correspond to the focus points mentioned in Tables II and IV. Vertical lines depict the 1-σ boundary for CDF [2] and D0 [3], respectively, as given in the text. The black point corresponds to the SM NNLO approximate value of at the LHC (165.2 pb) and the Tevatron (7.2 pb) [4].

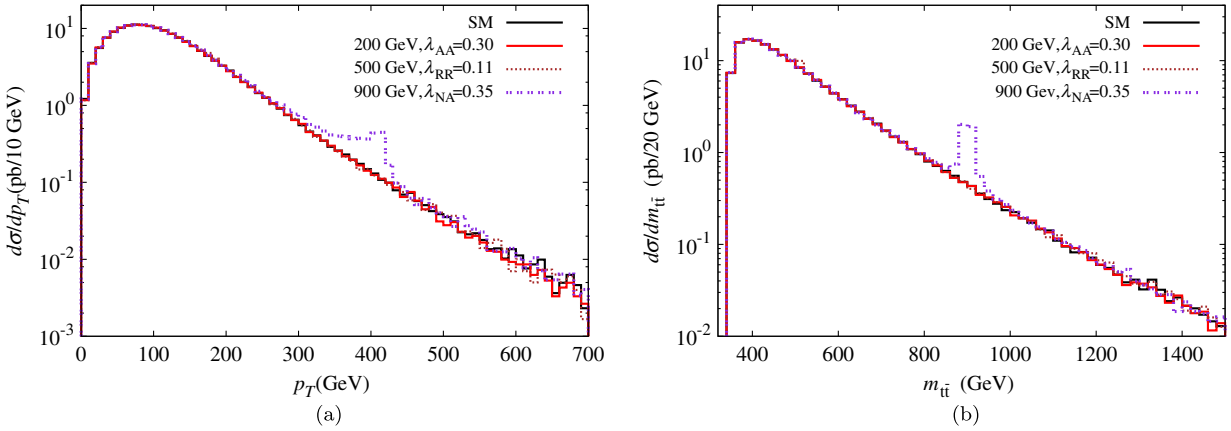

FIG. 18 (color online). The differential distribution of (a) transverse momentum of the top p_T with bin width 10 GeV and (b) top-pair invariant mass with bin width 20 GeV at the LHC with $\sqrt{s} = 7$ TeV corresponding to the SM and the flavor conserving focus points mentioned in Table II.

Unlike the Tevatron, the LHC possess a rich potential for the new physics resonant searches both for the threshold and the boosted production of the unlike sign top pairs. The differential cross sections for the $t\bar{t}$ production are studied in Ref. [54] along with Z' and other new physics resonant searches in Ref. [55]. No significant deviations from the SM are observed. We investigated the one dimensional distribution of the transverse momentum of the top and the invariant mass of the top pairs. Any large deviation that might occur due to the color-octet contribution in these distributions will exclude the corresponding resonant mass and the couplings. In Figs. 18(a) and 18(b) we show p_T and $m_{t\bar{t}}$ distribution at the LHC for the preferred values of parameters required to obtain the experimentally observed $A_{\rm FB}^{t\bar{t}}$. The p_T distribution as well as the $t\bar{t}$ invariant mass distribution for 7 TeV LHC data show a clear narrow resonance for $M_{V_8} = 900$ GeV on top of the SM background. Since ATLAS and CMS [54,55] have not yet observed any kind of such resonance effect for the p_T and $m_{t\bar{t}}$ distribution, the octet vector boson model with $M_{V_8} = 900$ GeV can be excluded with the coupling constant of 0.35.

In the flavor violation case $t\bar{t}$ production proceeds through V_8^0 exchange in the t channel and therefore no resonance effect is expected.

B. Charge asymmetry and spin correlation

We found that the $t\bar{t}$ production data at the Tevatron shows a relatively large $A_{\rm FB}^{t\bar{t}}$; the LHC data on the other hand exhibits a small "charge asymmetry" A_C given by

$$A_C = \frac{N(\Delta|y| > 0) - N(\Delta|y| < 0)}{N(\Delta|y| > 0) + N(\Delta|y| < 0)}, \qquad (21)$$

where $\Delta|y| = |y_t| - |y_{\bar{t}}|$ is the difference between absolute rapidities of the top and antitop quarks. In the SM both the asymmetries $A_{\rm FB}^{t\bar{t}}$ and A_C are generated at the NLO of QCD. The most recent results from the CMS [56] and ATLAS [57] collaborations at the LHC give $A_C^{\rm ATLAS} = -1.9 \pm 2.8(\text{stat}) \pm 2.4(\text{syst})\%$ and $A_C^{\rm CMS} = -1.3 \pm 2.8(\text{stat})^{+2.9}_{-3.1}(\text{syst})\%$. These values are consistent with the SM prediction, $A_C = 1.15 \pm 0.06\%$ within the experimental uncertainty [58].

Both the asymmetries depend on the coupling of color vector bosons with light and top quarks, i.e., on the $q\bar{q} \to t\bar{t}$ process. We provide a scatter plots in Figs. 19(a) and 19(b) in order to study the correlation between $A_{\rm FB}^{t\bar{t}}$ at the Tevatron and A_C at the LHC for three different vector boson masses corresponding to FC and FV interactions. In these figures x and y coordinates depict the $A_{\rm FB}^{t\bar{t}}$ in the Tevatron and A_C at the LHC, respectively, for a fixed value of the resonant mass and the coupling. The range of the couplings on the x axis is chosen such that it generates the appropriate $A_{\rm FB}^{t\bar{t}}$ observed in the $t\bar{t}$ production at the Tevatron. The favorable points mentioned in Tables II and IV are encircled in the figure. The inner and outer pair of vertical lines corresponds to the 1- and 2-σ boundaries of the experimental forward-backward asymmetry at the Tevatron [7] while horizontal line shows the 1-σ boundary of the experimental charge asymmetry at the LHC [56].

The LHC provides a unique platform to study the spin and polarization distribution of top and antitop for both the threshold and boosted events. We study and compare the contribution of the color octets to the spin-correlation coefficient $C^{t\bar{t}}$. To constrain the parameter space we plot the curves in the Figs. 20(a) and 20(b) for the flavor conserving and violating cases, respectively. Each point (x, y) on the curve estimates the contribution to $C^{t\bar{t}}$ at the Tevatron and the LHC, respectively, corresponding to a fixed value of the resonant mass and the coupling. The vertical and the horizontal lines depicts the experimental central values of $C^{t\bar{t}}$ at the Tevatron and the LHC, respectively. We observe that our focus points which are highlighted in the figure are in good agreement with the experimental values within 1σ error estimations.

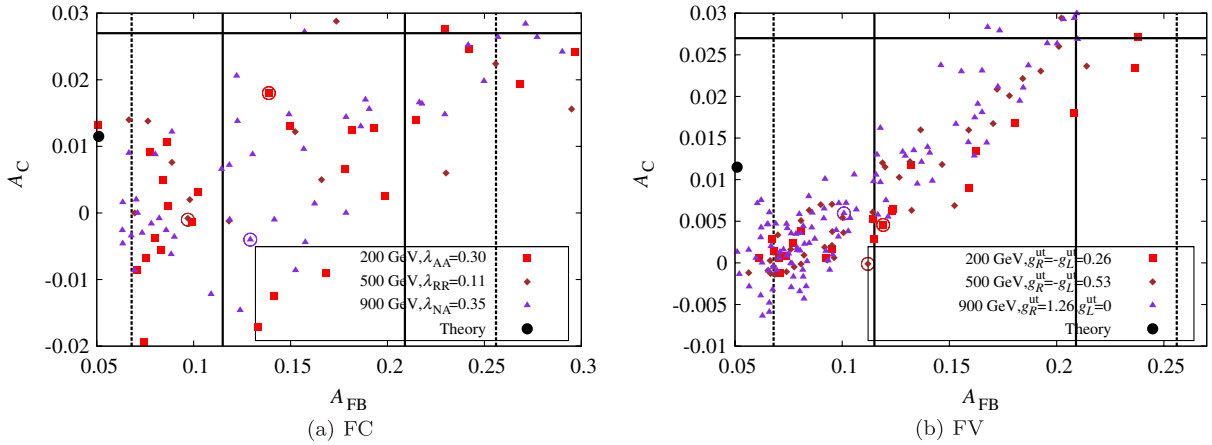

(a) FC (b) FV

FIG. 19 (color online). The x and y coordinates of the points in the scatter plot depict the $A_{FB}^{t\bar{t}}$ at the Tevatron and A_C at the LHC, respectively, corresponding to a fixed value of the coupling and the resonant mass for (a) flavor conserving and (b) flavor violating cases. The encircled colored data points corresponds to the focus points mentioned in Tables II and IV. The inner and outer pair of vertical lines are 1- and 2-σ boundaries of the experimental forward-backward asymmetry at the Tevatron [7] while horizontal line shows the 1-σ boundary of the experimental charge asymmetry at the LHC [56].

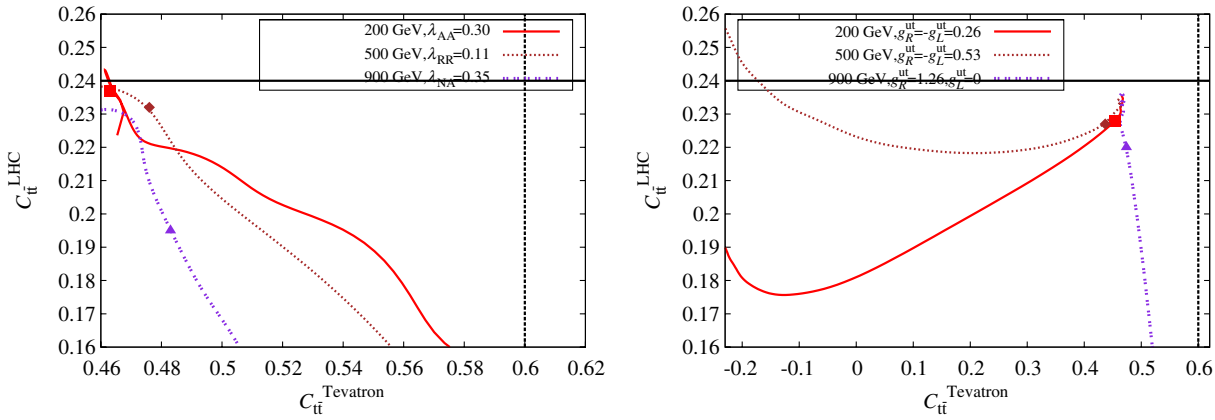

(a) FC (b) FV

FIG. 20 (color online). The x and y coordinates on the curve depicts the spin-correlation coefficients $C^{t\bar{t}}$ at the Tevatron and the LHC, respectively, corresponding to a fixed value of the coupling and the resonant mass for (a) flavor conserving and (b) flavor violating cases. The highlighted colored data points corresponds to the focus points mentioned in Tables II and IV. The horizontal and vertical lines corresponds to the central values of $C^{t\bar{t}}$ in the helicity basis at the LHC [59] and the Tevatron [43], respectively.

C. Dijet resonance searches

Recent searches for dijet resonances in 7 TeV pp collisions at ATLAS and CMS [36] provide exclusion limits for axigluon/coloron masses. CMS data exclude axigluons and colorons with mass less than 2.47 TeV at 95% confidence level while ATLAS exclusion limits are between 0.60 and 2.10 TeV for the same resonances. The color-octet vector bosons produced from the $q\bar{q}$ initial state will give rise to dijet events by decaying into the $q\bar{q}$ states. The dijet cross section thus depends on the same parameters namely M_{V_8}, Γ_{V_8}, g_L^q and g_R^q as the other observables considered in the study. Whereas the $t\bar{t}$ cross section depends on the product of the couplings of the color-octet vector bosons with light and top quarks g_i^q $g_j^t(i,j = L,R)$, the dijet cross section depends only on $(g_{L/R}^q)^2$ and therefore can provide a more stringent bounds on these couplings from the direct resonant searches. As discussed in the Introduction, the CMS and ATLAS collaborations have performed a search of narrow dijet resonances. The dijet resonance searches are based on the narrow width approximation and therefore they do not constraint vector bosons with large width.

We study the p_T distribution of the jet with highest p_T and invariant mass distribution of the two highest p_T jets in the SM and then compare the distribution with the specific choices of resonant mass along with their couplings as mentioned in Table II for the flavor conserving case. It is

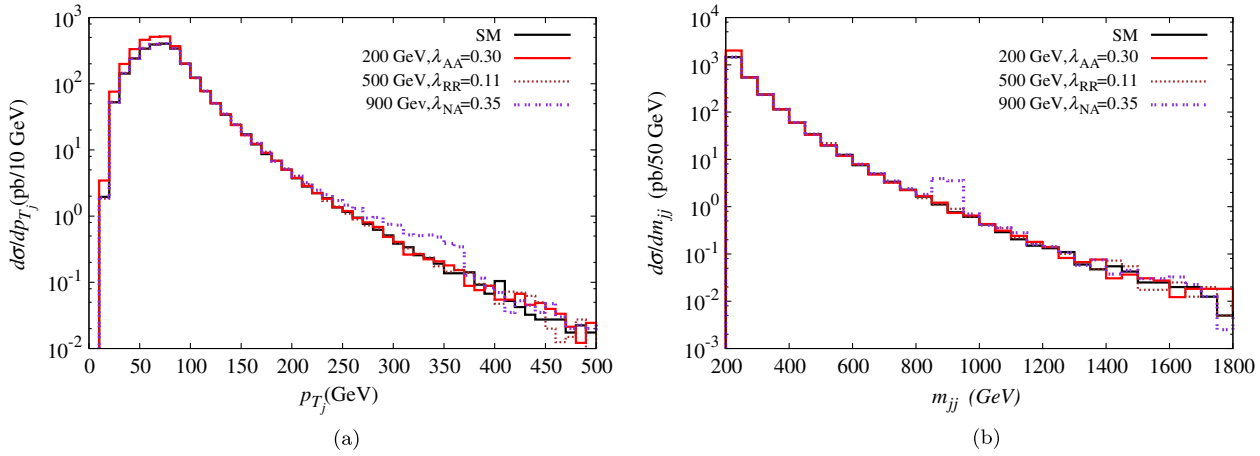

FIG. 21 (color online). The differential distribution of (a) transverse momentum of the highest p_T jet with bin width 10 GeV and (b) dijet invariant mass m_{jj} of the two highest p_T jets with bin width 50 GeV at the LHC with $\sqrt{s} = 7$ TeV corresponding to the SM and the focus points mentioned in Table II for flavor conserving case.

to be noted that there is no contribution from flavor violating couplings involving the first and third generation quarks.

We have imposed the standard acceptance cuts for these distributions. The minimum dijet invariant mass m_{jj} is taken to be 200 GeV along with the required pseudorapidity separation $|\Delta\eta| \leq 1.3$ and both jets satisfying $|\eta| \leq 2.5$. We show the p_T distribution in Fig. 21(a) with the bin width 10 GeV and the invariant mass distribution of the two highest p_T jets in Fig. 21(b) with bin width 50 GeV.

The $d\sigma/dm_{jj}$ distribution are all in good agreement with the SM QCD background within the experimental error bars except for the case of $M_{V_8} = 900$ GeV. Therefore the $M_{V_8} = 900$ GeV resonance can be excluded based on the resonant searches not only from the $t\bar{t}$ production but also from the dijet searches as well.

VII. SUMMARY AND CONCLUSION

We have revisited and extended the analysis of the color-octet vector boson model in the top sector at the Tevatron and the LHC for FC and FV couplings. We have considered the effect of decay width of the color-octet vector bosons throughout our analysis and configured our study to constrain the parameter space of the model from the observed differential distribution of the forward-backward asymmetry with 8.7 fb^{-1} full data set of the CDF collaboration at the Tevatron [7] and charge asymmetry data set from the LHC at 7 TeV [56], which was missing in the literature [22,31,32]. We have made an attempt to find a parameter space which is also consistent with the spin-correlation observation at the Tevatron [43,44], single top production at the Tevatron [13], same-sign top production at the Tevatron [16] and the LHC [17,18] and dijet invariant mass distribution at the LHC [36]. The observed features of our analysis for top quark physics at the Tevatron and the LHC are enumerated as follows:

(1) We notice an appreciable contribution to $A_{\rm FB}^{t\bar{t}}$ and a spin-correlation coefficient from the axial current and the right-handed chiral current without transgressing the production cross sections within the experimentally allowed one sigma region.

(2) We scanned the parameter space of the model to explain the anomaly observed in one dimensional $m_{t\bar{t}}$ and $|\Delta y|$ distributions of $A_{\rm FB}^{t\bar{t}}$. We predict few focus points based on the χ^2 minimization at $\chi^2_{\rm min}$ which are likely to satisfy these constraints. This is summarized in Tables II and III and in Tables IV and V for the flavor conserving and flavor changing neutral currents, respectively. $m_{t\bar{t}}$ distribution of $A_{\rm FB}^{t\bar{t}}$ corresponding to focus points are also depicted in Figs. 8(a), 8(c), 8(e), 9(a), 9(c), and 9(e) for FC and FV couplings, respectively. Similarly the agreement with respect to $|\Delta y|$ distribution is shown in Figs. 8(b), 8(d), 8(f), 9(b), 9(d), and 9(f) for flavor conserving and violating cases, respectively.

(3) We verified that the top quark couplings corresponding to these focus points evade the lower bounds on the chiral couplings required to form top quark condensates [35].

(4) Single top quark production through a massive color charged vector boson is studied for the s and t channels separately with distinguishable final states as in the SM. We observe that a large parameter region is allowed by the one and two sigma bands corresponding to s and t channels, respectively, from the CDF [13]. Since we have performed our analysis with $|V_{tb}|^2 = 1$, we need to be careful about the interplay of new physics parameters and allowed deviation for $|V_{tb}|$ from unity.

(5) The introduction of a flavor changing neutral current for the $t\bar{t}$ production also induces the single top production in s and t channels with the same final states. So, we compared our results with the

observed combined cross sections from s and t channels at the Tevatron. We find that the cross section of the single top quark production is comparatively more sensitive to the new physics couplings in comparison to the $t\bar{t}$ model. We are able to constrain the product of FC and FV couplings of the neutral current from this process.

As discussed in Sec. II, the inclusion of nonuniversal couplings in the up quark sector help the product of flavor violating couplings to evade the low energy stringent bounds from B and D physics. The benchmark points obtained by us are consistent with all the observables discussed above and are in broad agreement with those obtained in Ref. [22].

(6) Consistency of the color-octet vector boson model with respect to focus points is examined in the light of recent LHC data in Sec. VI. We probed the admissibility of the constrained parameter space at the LHC which explained the required $A_{\rm FB}^{t\bar{t}}$ at the Tevatron as mentioned in Sec. III C. We observe that the focus points do not transgress the cross section of the top-pair production [53] as well as the measured charge asymmetry [56] and spin correlation [59] at the LHC.

To have more insight on the implication of the new physics parameter space we study the p_T and $m_{t\bar{t}}$ distributions of the top pair. We find that all our FC focus points as mentioned in Table II except for the higher resonance mass of 900 GeV are consistent with the observations at the LHC.

The correlation study of the $A_{\rm FB}^{t\bar{t}}$ at the Tevatron and A_C at the LHC in Figs. 19(a) and 19(b) shows that the large $A_{\rm FB}^{t\bar{t}}$ at the Tevatron can be accommodated by the recent observations at the LHC within a 2-σ limit. The spin-correlation coefficient predicted with constrained parameter space of the color excited states at the LHC are also found to lie within the one-σ limit of the experimental values [43,59].

(7) The ballpark estimate of the production cross sections of the color exotics involving the light quark color-octet vector interactions are given in Table I. Since the strongest bound for the light quark couplings to the color exotics comes from the dijet searches, we studied the transverse momentum and invariant dijet mass distribution at the LHC corresponding to the parameter space which generated a large $A_{\rm FB}^{t\bar{t}}$ at the Tevatron. We observe an appreciable deviation for the color octet at 900 GeV similar to that observed for $m_{t\bar{t}}$ distribution.

(8) We also studied the production cross section of same-sign top and antitop pairs via FV couplings at the Tevatron. We imposed the constraints of nonobservability of large same-sign dilepton events at the Tevatron and provided the 95% exclusion contours in Fig. 16(a) on the plane of chiral couplings. Exclusion contours at 95% are also computed from recent results at CMS and ATLAS for the same-sign top production only which are depicted in Figs. 16(b) and 16(c), respectively. The constraints from the LHC restrict the allowed parameter space of FV to a narrow allowed region. We observe that all focus points except one (900 GeV with $g_R^{ut} = 1.26$) corresponding to FV couplings as shown in Fig. 16(c) lies within this narrow allowed region.

Our analysis for the top quark physics in the vector color-octet model based on the recent observations at the Tevatron and the LHC has shrunk the allowed parameter space to a great extent. We propose four focus data points (two each from flavor conserving and violating couplings) which can explain the $A_{\rm FB}^{t\bar{t}}$ anomaly at the Tevatron and are also consistent with the $t\bar{t}$, same-sign top and dijet production cross sections and associated observables at the LHC.

ACKNOWLEDGMENTS

The authors would like to thank Amitabha Mukherjee, Debajyoti Choudhury, Mamta Dahiya, and Rashidul Islam for fruitful discussions. S. D. and M. K. thank Fabio Maltoni and Rikkert Frederix for illuminating discussions on MadGraph and single top analysis. We acknowledge the partial support from DST, India under Grant No. SR/S2/HEP-12/2006. S. D. and A. G. would like to acknowledge the UGC research award and CSIR(ES) award, respectively, for the partial financial support. We also thank RECAPP, HRI for local hospitality where part of the work was done.

APPENDIX: COMPUTATION OF HELICITY AMPLITUDES

1. Helicity amplitudes for $q\bar{q} \to t\bar{t}$ via flavor conserving vector octets

All couplings are in units of g_s. $g_L^q = g_L^t = g_R^q = g_R^t = 1$ for SM,

$$\mathcal{M}^{V_8^0}_{+-\pm\pm} = \mathcal{F}_s g_R^q (g_L^t + g_R^t) \frac{\hat{s}}{2} \sqrt{1-\beta^2} \sin\theta = \mathcal{M}^{V_8}_{-+\mp\mp}(L \leftrightarrow R, R \leftrightarrow L), \tag{A1}$$

$$\mathcal{M}^{V_8^0}_{+-\pm\mp} = \mathcal{F}_s g_R^q [(g_L^t + g_R^t) \mp \beta (g_L^t - g_R^t)] \frac{\hat{s}}{2} (1 \pm \cos\theta) = \mathcal{M}^{V_8}_{-+\mp\pm}(L \leftrightarrow R, R \leftrightarrow L), \tag{A2}$$

where

$$\mathcal{F}_s = \frac{g_s^2 T^a T^a}{(\hat{s} - M^2_{V_8^0}) + i M_{V_8^0} \Gamma_{V_8^0}},$$

and T^a are the SU(3) matrices.

2. Helicity amplitudes for $q\bar{q} \to t\bar{t}$ via flavor violating vector octets

$$\mathcal{M}^{V_8}_{++\pm\pm} = \mathcal{F}_t g_R^{ut} g_L^{ut} \hat{s}(1 \pm \beta) = \mathcal{M}^{V_8}_{--\mp\mp}(L \leftrightarrow R, R \leftrightarrow L), \quad \text{(A3)}$$

$$\mathcal{M}^{V_8}_{+-\pm\pm} = \mathcal{F}_t g_R^{ut2} \frac{\hat{s}}{2}\sqrt{1-\beta^2}\sin\theta = \mathcal{M}^{V_8}_{-+\pm\pm}(L \leftrightarrow R, R \leftrightarrow L), \quad \text{(A4)}$$

$$\mathcal{M}^{V_8}_{+-\pm\mp} = \mathcal{F}_t g_R^{ut2} \frac{\hat{s}}{2}(1 \pm \beta)(1 \pm \cos\theta) = \mathcal{M}^{V_8}_{-+\mp\pm}(L \leftrightarrow R, R \leftrightarrow L), \quad \text{(A5)}$$

where

$$\mathcal{F}_t = \frac{g_s^2 T^a T^a}{(\hat{t} - M^2_{V_8^0}) + iM_{V_8^0}\Gamma_{V_8^0}}.$$

[1] Tevatron Electroweak Working Group, CDF Collaboration, and D0 Collaboration, arXiv:1007.3178.
[2] CDF Collaboration, CDF Conference Note 9913.
[3] V. M. Abazov *et al.* (D0 Collaboration), Phys. Lett. B **704**, 403 (2011).
[4] N. Kidonakis, arXiv:1205.3453; Phys. Rev. D **82**, 114030 (2010); arXiv:1105.3481; arXiv:0909.0037.
[5] CDF Collaboration, Phys. Rev. D **83**, 112003 (2011); CDF Collaboration, CDF Conference Note 10436; CDF Collaboration, CDF Conference Note 10584.
[6] V. M. Abazov *et al.* (D0 Collaboration), Phys. Rev. D **84**, 112005 (2011).
[7] CDF Collaboration, arXiv:1211.1003 [Phys. Rev. D (to be published)]; CDF Collaboration, CDF Conference Note 10807.
[8] S. Frixione, P. Nason, and G. Ridolfi, J. High Energy Phys. 09 (2007) 126; N. Kidonakis, Phys. Rev. D **84**, 011504 (2011); V. Ahrens, A. Ferroglia, M. Neubert, B. D. Pecjak, and L. L. Yang, Phys. Rev. D **84**, 074004 (2011); W. Hollik and D. Pagani, Phys. Rev. D **84**, 093003 (2011); J. Kühn and G. Rodrigo, J. High Energy Phys. 01 (2012) 063; A. V. Manohar and M. Trott, Phys. Lett. B **711**, 313 (2012).
[9] M. Dahiya, S. Dutta, and R. Islam, Phys. Rev. D **86**, 115022 (2012).
[10] J. Shu, K. Wang, and G. Zhu, Phys. Rev. D **85**, 034008 (2012); M. I. Gresham, I.-W. Kim, and K. M. Zurek, Phys. Rev. D **83**, 114027 (2011); D. Duffy, Z. Sullivan, and H. Zhang, Phys. Rev. D **85**, 094027 (2012); M. I. Gresham, I.-W. Kim, and K. M. Zurek, Phys. Rev. D **83**, 114027 (2011).
[11] J. A. Aguilar-Saavedra and M. Perez-Victoria, J. High Energy Phys. 09 (2011) 097; Phys. Rev. D **84**, 115013 (2011).
[12] See, e.g., the following and references therein: Q.-H. Cao, D. McKeen, J. L. Rosner, G. Shaughnessy, and C. E. M. Wagner, Phys. Rev. D **81**, 114004 (2010).
[13] CDF Collaboration, CDF Conference Note 10793.
[14] V. M. Abazov *et al.* (D0 Collaboration), Phys. Rev. D **84**, 112001 (2011).
[15] CMS Collaboration, Report No. CMS-PAS-TOP-10-008.
[16] CDF Collaboration, CDF Conference Note 10466.
[17] CMS Collaboration, J. High Energy Phys. 08 (2011) 005.
[18] ATLAS Collaboration, J. High Energy Phys. 04 (2012) 069.
[19] S. Jung, H. Murayama, A. Pierce, and J. D. Wells, Phys. Rev. D **81**, 015004 (2010).
[20] K. Cheung, W.-Y. Keung, and T.-C. Yuan, Phys. Lett. B **682**, 287 (2009).
[21] K. Agashe, A. Belyaev, T. Krupovnickas, G. Perez, and J. Virzi, Phys. Rev. D **77**, 015003 (2008); B. Lillie, L. Randall, and L. T. Wang, J. High Energy Phys. 09 (2007) 074; B. Lillie, J. Shu, and T. M. P. Tait, Phys. Rev. D **76**, 115016 (2007).
[22] B. Grinstein, A. L. Kagan, J. Zupan, M. Trott, and J. Zupan, J. High Energy Phys. 10 (2011) 072.
[23] For SUSY R-parity violating interactions, see a review R. Barbier *et al.*, Phys. Rep. **420**, 1 (2005), and references therein.
[24] N. Cabibbo, L. Maiani, and Y. Srivastava, Phys. Lett. **139B**, 459 (1984); A. De Rujula, L. Maiani, and R. Petronzio, Phys. Lett. **140B**, 253 (1984); J. H. Kuhn and P. M. Zerwas, Phys. Lett. **147B**, 189 (1984).
[25] U. Baur, I. Hinchliffe, and D. Zeppenfeld, Int. J. Mod. Phys. A **02**, 1285 (1987); U. Baur, M. Spira, and P. M. Zerwas, Phys. Rev. D **42**, 815 (1990).
[26] J. L. Hewett and T. G. Rizzo, Phys. Rep. **183**, 193 (1989).
[27] B. A. Dobrescu, K. Kong, and R. Mahbubani, J. High Energy Phys. 07 (2007) 006; B. A. Dobrescu, K. Kong, and R. Mahbubani, Phys. Lett. B **670**, 119 (2008).
[28] J. Shu, T. M. P. Tait, and K. Wang, Phys. Rev. D **81**, 034012 (2010); A. Arhrib, R. Benbrik, and C.-H. Chen, Phys. Rev. D **82**, 034034 (2010); Z. Ligeti, G. M. Tavares, and M. Schmaltz, J. High Energy Phys. 06 (2011) 109; I. Dorsner, S. Fajfer, J. F. Kamenik, and N. Kosnik, Phys. Rev. D **81**, 055009 (2010); J. C. Pati and A. Salam, Phys. Rev. D **10**, 275 (1974); **11**, 703(E) (1975); R. N. Mohapatra and R. E. Marshak, Phys. Rev. Lett. **44**, 1316 (1980); **44**, 1643(E) (1980); Z. Chacko and R. N. Mohapatra, Phys. Rev. D **59**, 055004 (1999).
[29] S. Cullen, M. Perelstein, and M. E. Peskin, Phys. Rev. D **62**, 055012 (2000); P. Burikham, T. Figy, and T. Han, Phys. Rev. D **71**, 016005 (2005); **71**, 019905(E) (2005)]; Z. Dong, T. Han, M. X. Huang, and G. Shiu, J. High Energy Phys. 09 (2010) 048; L. A. Anchordoqui, H. Goldberg, and T. R. Taylor, Phys. Lett. B **668**, 373

(2008); L. A. Anchordoqui, H. Goldberg, D. Lust, S. Nawata, S. Stieberger, and T. R. Taylor, Phys. Rev. Lett. **101**, 241803 (2008).
[30] C. T. Hill and E. H. Simmons, Phys. Rep. **381**, 235 (2003); **390**, 553(E) (2004), and references therein.
[31] G. Z. Krnjaic, Phys. Rev. D **85**, 014030 (2012); D. Choudhury, R. M. Godbole, S. D. Rindani, and P. Saha, Phys. Rev. D **84**, 014023 (2011); P. Ferrario and G. Rodrigo, Phys. Rev. D **80**, 051701 (2009); P. H. Frampton, J. Shu, and K. Wang, Phys. Lett. B **683**, 294 (2010); P. H. Frampton and S. L. Glashow, Phys. Lett. B **190**, 157 (1987); J. Bagger, C. Schmidt, and S. King, Phys. Rev. D **37**, 1188 (1988); J. A. Aguilar-Saavedra and M. Perez-Victoria, Phys. Lett. B **705**, 228 (2011); A. R. Zerwekh, Eur. Phys. J. C **65**, 543 (2010); Phys. Lett. B **704**, 62 (2011); R. S. Chivukula, E. H. Simmons, and C.-P. Yuan, Phys. Rev. D **82**, 094009 (2010); G. Marques Tavares and M. Schmaltz, Phys. Rev. D **84**, 054008 (2011).
[32] H. Wang, Y.-K. Wang, B. Xiao, and S.-h. Zhu, Phys. Rev. D **84**, 094019 (2011).
[33] X.-P. Wang, Y.-K. Wang, B. Xiao, J. Xu, and S.-h. Zhu, Phys. Rev. D **83**, 115010 (2011).
[34] J. Sayre, D. A. Dicus, C. Kao, and S. Nandi, Phys. Rev. D **84**, 015011 (2011); D. A. Dicus, C. Kao, S. Nandi, and J. Sayre, Phys. Rev. D **83**, 091702 (2011); I. Bertram and E. H. Simmons, Phys. Lett. B **443**, 347 (1998); E. H. Simmons, Phys. Rev. D **55**, 1678 (1997); A. Atre, R. S. Chivukula, P. Ittisamai, E. H. Simmons, and J.-H. Yu, Phys. Rev. D **86**, 054003 (2012); H. X. Zhu, C. S. Li, D. Y. Shao, J. Wang, and C. P. Yuan, Eur. Phys. J. C **72**, 2232 (2012); R. S. Chivukula, A. Farzinnia, E. H. Simmons, and R. Foadi, Phys. Rev. D **85**, 054005 (2012); L. M. Carpenter and S. Mantry, Phys. Lett. B **703**, 479 (2011); B. Xiao, Y.-K. Wang, and S.-h. Zhu, arXiv:1011.0152; A. R. Zerwekh, Eur. Phys. J. C **70**, 917 (2010).
[35] C. T. Hill, Phys. Lett. B **266**, 419 (1991); C. T. Hill and S. J. Parke, Phys. Rev. D **49**, 4454 (1994); R. S. Chivukula, A. G. Cohen, and E. H. Simmons, Phys. Lett. B **380**, 92 (1996).
[36] CMS Collaboration, Phys. Lett. B **704**, 123 (2011); ATLAS Collaboration, Phys. Rev. Lett. **105**, 161801 (2010).
[37] T. Han, I. Lewis, and Z. Liu, J. High Energy Phys. 12 (2010) 085.
[38] Y. Bai, J. L. Hewett, J. Kaplan, and T. G. Rizzo, J. High Energy Phys. 03 (2011) 003.
[39] U. Haisch and S. Westhoff, J. High Energy Phys. 08 (2011) 088.
[40] J. Alwall, P. Demin, S. de Visscher, R. Frederix, M. Herquet, F. Maltoni, T. Plehn, D. L. Rainwater, and T. Stelzer, J. High Energy Phys. 09 (2007) 028.
[41] O. Antunano, J. H. Kuhn, and G. Rodrigo, Phys. Rev. D **77**, 014003 (2008); M. T. Bowen, S. D. Ellis, and D. Rainwater, Phys. Rev. D **73**, 014008 (2006); S. Dittmaier, P. Uwer, and S. Weinzierl, Phys. Rev. Lett. **98**, 262002 (2007).
[42] W. Bernreuther and Z.-G. Si, Nucl. Phys. **B837**, 90 (2010).
[43] CDF Collaboration, Phys. Rev. D **83**, 031104 (2011).
[44] CDF Collaboration, CDF Conference Note 10719, http://www-cdf.fnal.gov/physics/new/top/2011//SpinCorrDIL/SpinCorrDIL_Pub/spincorrPubnote.pdf; V. M. Abazov *et al.* (D0 Collaboration), Phys. Lett. B **702**, 16 (2011).
[45] P. Ko, Y. Omura, and C. Yu, Nuovo Cimento Soc. Ital. Fis. C **035N3**, 245 (2012); D.-W. Jung, P. Ko, J. S. Lee, and S.-h. Nam, Phys. Lett. B **691**, 238 (2010); D.-W. Jung, P. Ko, and J. S. Lee, Phys. Lett. B **701**, 248 (2011); **708**, 157 (2012); Phys. Rev. D **84**, 055027 (2011); P. Ko, Y. Omura, and C. Yu, Phys. Rev. D **85**, 115010 (2012); J. High Energy Phys. 01 (2012) 147; Eur. Phys. J. C **73**, 2269 (2013).
[46] C. Kao, Phys. Lett. B **348**, 155 (1995); C.-S. Li, R. J. Oakes, J. M. Yang, and C. P. Yuan, Phys. Lett. B **398**, 298 (1997); S. Gopalakrishna, T. Han, I. Lewis, Z.-g. Si, and Y.-F. Zhou, Phys. Rev. D **82**, 115020 (2010); R. M. Godbole, K. Rao, S. D. Rindani, and R. K. Singh, J. High Energy Phys. 11 (2010) 144; C. Kao and D. Wackeroth, Phys. Rev. D **61**, 055009 (2000); K.-i. Hikasa, J. M. Yang, and B.-L. Young, Phys. Rev. D **60**, 114041 (1999); P.-Y. Li, G.-R. Lu, J. M. Yang, and H. Zhang, Eur. Phys. J. C **51**, 163 (2007); J. Cao, L. Wu, and J. M. Yang, Phys. Rev. D **83**, 034024 (2011).
[47] D. Chang, S.-C. Lee, and A. Soumarokov, Phys. Rev. Lett. **77**, 1218 (1996); S. Fajfer, J. F. Kamenik, and B. Melic, J. High Energy Phys. 08 (2012) 114.
[48] G. L. Kane, G. A. Ladinsky, and C. P. Yuan, Phys. Rev. D **45**, 124 (1992).
[49] M. Arai, N. Okada, K. Smolek, and V. Simak, Phys. Rev. D **75**, 095008 (2007).
[50] J. M. Campbell, R. Frederix, F. Maltoni, and F. Tramontano, Phys. Rev. Lett. **102**, 182003 (2009).
[51] J. M. Campbell, R. Frederix, F. Maltoni, and F. Tramontano, J. High Energy Phys. 10 (2009) 042.
[52] F. Maltoni, G. Ridolfi, and M. Ubiali, J. High Energy Phys. 07 (2012) 022; 04 (2013) 095(E).
[53] ATLAS Collaboration, Report No. ATLAS-CONF-2012-134.
[54] CMS Collaboration, Eur. Phys. J. C **73**, 2339 (2013); J. High Energy Phys. 12 (2012) 015.
[55] CMS Collaboration, Phys. Rev. D **87**, 072002 (2013); ATLAS Collaboration, J. High Energy Phys. 01 (2013) 116; 09 (2012) 041; Eur. Phys. J. C **72**, 2083 (2012).
[56] CMS Collaboration, Phys. Lett. B **709**, 28 (2012).
[57] ATLAS Collaboration, Eur. Phys. J. C **72**, 2039 (2012).
[58] J. H. Kuhn and G. Rodrigo, J. High Energy Phys. 01 (2012) 063.
[59] CMS PAS TOP-12-004; ATLAS Collaboration, Phys. Rev. Lett. **108**, 212001 (2012).